Geology of Ore Deposits, Vol. 45, No. 6, 2003, pp. 423–451. Translated from Geologiya Rudnykh Mestorozhdenii, Vol. 45, No. 6, 2003, pp. 483–513.

Effect of Radiation on Properties of Confinement Matrices for Immobilization of Actinide-Bearing Wastes

N. P. Laverov*, S. V. Yudintsev*,[1] T. S. Yudintseva*, S. V. Stefanovsky, R. C. Ewing***, J. Lian***, S. Utsunomiya***, and L. M. Wang*****

**Institute of Geology of Ore Deposits, Petrography, Mineralogy, and Geochemistry, Russian Academy of Sciences, Staromonetnyi per. 35, Moscow, 119017 Russia*

***State Unitary Enterprise of Moscow—Joint Environmental, Technological, and Research Center for Radioactive Waste Immobilization and Environmental Protection (Mos NPO Radon), 7 Rostovskii per. 2/14, Moscow, 119121 Russia*

****Department of Nuclear Engineering and Radiological Sciences, University of Michigan, Ann Arbor, MI, 48109-2104 USA*

Received March 12, 2003

Abstract—Structural damage to actinide-bearing matrices upon their irradiation with Kr and Xe ions with energies of 1.0 and 1.5 MeV was studied. Actinides are incorporated into oxides with fluorite-type structures (zirconolite, pyrochlore, and murataite), uranium titanate (brannerite), silicates and ferrites with a garnet lattice, and a (Ca, REE) silicate with an apatite structure (britholite). The radiation doses for complete structural amorphization at 25°C were as follows (in units of 10^{14} ions/cm^2): 2.9 for zirconolite, 1.8–2.4 for pyrochlore, 1.5–2 for garnet, 1.7–1.9 for murataite, 1.4 for brannerite, and 0.4 for britholite. The radiation resistance of phases expressed as the number of displacements per atom (dpa) ranges from 0.1 to 0.4 dpa. According to these data, a phase containing 10 wt % ^{239}Pu will be completely amorphized over 500–2000 yr. This will increase actinide leaching from the matrix by tens of times. Amorphization doses are several times higher for natural analogues because of healing of radiation damage to the mineral structure with time. Disposal of highly radioactive waste matrices in deep-well repositories with an elevated temperature of ambient rocks favors an increase in the resistance of the crystal structure to radiation and maintains the immobilizing properties of radionuclide-bearing matrices over longer periods.

INTRODUCTION

The development of efficient techniques for management of high-level radioactive wastes (HLW) of nuclear power engineering is an important scientific problem. One solution suggests incorporation of these HLW into special materials, confinement matrices, capable of long-term isolation of radionuclides from the environment. It is particularly important to develop matrices for long-lived actinides with half-lives from hundreds (^{241}Am) to tens of thousands (^{239}Pu) and millions (^{237}Np) of years. These radionuclides are very toxic and hazardous for the biosphere. An example of wastes with high actinide contents (tens of weight percent) is the actinide fraction of liquid HLW from conversion of weapons plutonium into nuclear fuel. Various crystalline phases capable of actinide incorporation and having high chemical resistance are proposed for their immobilization (Hench *et al.*, 1984; Ringwood, 1985; Fielding and White, 1987; *Radioactive …,* 1988). The following oxides with fluorite-type structures are the most promising among actinide matrices: zirconolite and pyrochlore (Vance *et al.*, 1995; Ewing *et al.*, 1996; Laverov *et al.*, 1996, 2001; Ebbinghaus *et al.*, 1998; Gong *et al.*, 1999; Stefanovsky *et al.*, 2001) and murataite (Laverov *et al.*, 1998$_1$, 1998$_2$, 1999; Stefanovsky *et al.*, 1999). The crystal lattices of these phases can incorporate a large amount of tri- and tetravalent actinides and neutron absorbers (Gd, Hf). The rate of U and Pu leaching from these phases ranges from 10^{-2} to 10^{-5} g/(m^2 day) (Burakov *et al.*, 2001; Weber and Ewing, 2002) and decreases with time. Alumoferrites with garnet structures can also serve as matrices for immobilization of actinide-bearing HLW with complex composition (Burakov and Anderson, 2000; Yudintsev, 2001, 2003; Yudintsev *et al.*, 2002). They can contain 20 wt % actinides, as well as their decay products (REE, Zr), many corrosion products, and various technological admixtures (Zr, Fe, Al, Ga, Si, etc.).

The properties of HLW matrices inevitably change with time because of radioactive decay of incorporated radionuclides. Destruction of the crystal lattice weakens bonds between atoms (including actinide atoms) and decreases the reliability of their immobilization in the matrix phase. This increases the solubility of matrices in aqueous solutions. The rate of actinide leaching from amorphized materials can increase by tens and hundreds of times as compared to the initial crystalline phases (Wald and Weber, 1984; Hart *et al.*, 1996; Matzke and van Geel, 1996; Burakov *et al.*, 2001; Weber and Ewing, 2002; Lukinykh *et al.*, 2002). Lattice destruction can also cause swelling (by 6–18%), accu-

[1]Corresponding author: S.V. Yudintsev. E-mail: syud@igem.ru

Table 1. Calculated irradiation doses in HLW-bearing glasses and crystalline matrices with weapons plutonium (Weber, 1991; Ewing, 1999)

Time, yr	Glass with 20 wt % HLW from conversion of irradiated nuclear fuel			1 wt % ^{239}Pu	10 wt % ^{239}Pu
	α decay events/g	β decay events/g	β and α irradiation, rad	α decay events/g	α-decay events/g
1	2×10^{14}	5×10^{16}	6×10^{8}	7×10^{14}	7×10^{15}
10	2×10^{15}	5×10^{17}	6×10^{9}	7×10^{15}	7×10^{16}
10^2	2×10^{16}	2×10^{18}	3×10^{10}	7×10^{16}	7×10^{17}
10^3	10^{17}	5×10^{18}	6×10^{10}	7×10^{17}	7×10^{18}
10^4	3×10^{17}	5×10^{18}	8×10^{10}	7×10^{18}	7×10^{19}
10^5	5×10^{17}	5×10^{18}	10^{11}	2×10^{19}	2×10^{20}
10^6	10^{18}	5×10^{18}	10^{11}	2.5×10^{19}	2.5×10^{20}

mulation of stored energy (50–150 J/g), transformation of one element to another (transmutation), formation of helium bubbles due to electron capture by α particles, and modification of the phase composition and physical properties of matrices (hardness and Young's modulus). All these processes affect the confinement properties of the matrices. For example, swelling leads to fracturing of grains, increases the area of their contact with groundwater, and consequently increases the rate of radionuclide leaching. Therefore, knowledge of the radiation-induced changes in the properties of actinide-bearing phases is very important for estimation of HLW matrix behavior during long-term disposal.

This problem has been addressed in special works (Weber and Roberts, 1983; Weber, 1991; Ewing *et al.*, 1995; Weber *et al.*, 1997, 1998; Weber and Ewing, 2002) summarizing data on the influence of radiation on glasses and crystal phases with zircon, zirconolite, pyrochlore, perovskite, and monazite structures. Similar reviews are absent in the Russian geological literature. We attempt to fill this gap with our paper and include new results on the radiation susceptibility of some promising actinide immobilization matrices and their natural mineral analogues.

RADIATION-INDUCED PROCESSES IN GLASS MATRICES

The main radiation in HLW matrices is produced by β- and α decay of fission products and actinides and γ radiation (Weber, 1991; Weber *et al.*, 1997). The γ radiation causes glass radiolysis and oxidation of nitrogen (gaseous or dissolved in contacting water). The latter process decreases the solution pH and increases the rate of element leaching from the solidified wastes. The decay of fission products (^{90}Sr, ^{137}Cs, etc.) generates β particles and low-energy recoil nuclei. Calculations show that this process is the main radiation source during the first several hundred years of storage of solidified HLW (Table 1). It is accompanied by high heat release and matrix heating to 200–400°C in correspondence with the fission product concentration (Weber *et al.*, 1997). However, the process does not affect the glass framework significantly.

The main mechanism of matrix destruction is actinide decay with emission of α particles and complementary heavy recoil nuclei. The α particles (He^{2+} ions with energies of 4.5–5.5 MeV) bear up to 98% of the decay energy, which is generally consumed for substance ionization. At the end of their tracks (10–20 μm), the α particle collide with several hundreds of atoms and cause their displacement. The heavy recoil nuclei have energies of 70–100 keV. They move over shorter distances (10–40 nm), but collide with a greater number of atoms (*Radioactive …*, 1988).

Radiation can cause glass expansion by no more than 1–2% (Weber, 1991; Weber *et al.*, 1997). Volume increases are observed for glass matrices with crystalline phases and for matrices with a low alkali/Si ratio. Radiation-induced changes in bonds between atoms lead to accumulation of excess energy, which is released as heat on a temperature increase. Generally, this energy does not exceed 150 J/g (normally being 100–130 J/g) and reaches its highest value at a dose of $(0.1–0.3) \times 10^{18}$ α decay events/g. Annealing of borosilicate glass for 7 days at 100°C decreases the excess energy by about 90% (as compared to room temperature), and its amount decreases to zero after annealing at 350°C (Weber and Roberts, 1983). The specific heat capacity of glasses is about 1 J/g. Thus, rapid release of excess energy can cause their heating to 50–125°C.

Decay is accompanied by transmutation, which is generally caused by β decay of ^{137}Cs and ^{90}Sr, which are very abundant in HLW. As a result, Cs turns into Ba^{2+}, with a 20% decrease in the ionic radius, while Sr (through the short-lived Y^{3+}) turns into Zr^{4+}, with an ionic radius 29% smaller than that of the initial Sr^{2+}. It was found that cesium transmutation does not significantly affect the microstructure and chemical resistance of glass matrices.

Helium forms by capture of two electrons by an α particle and is accumulated in interstices and defects as bubbles 200–300 nm in diameter. Heating of irradi-

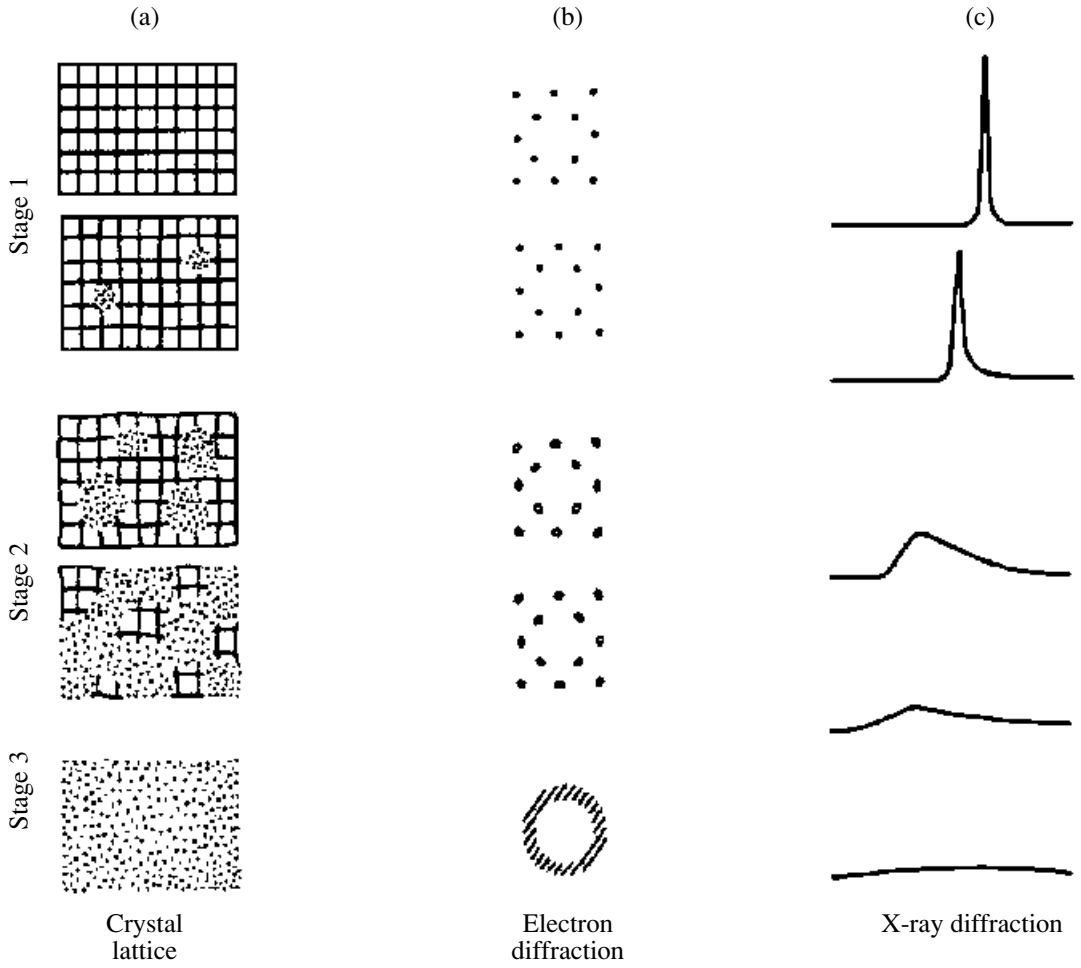

Fig. 1. Schemes of structural changes (a) and electron (b) and X-ray (c) diffraction patterns with increasing irradiation dose (Murakami *et al.*, 1991; Ewing *et al.*, 1995).

ated glasses accelerates the bubble formation. The glass decomposition induced by γ irradiation can cause the formation of oxygen-filled bubbles. Changes in the glass microstructure are primarily expressed in its heterogenization, including formation of new phases and microfissuring. For glasses with ^{238}Pu and ^{244}Cm, the glass hardness and Young's modulus decrease exponentially with increasing irradiation dose, with the maximum changes being 25 and 30%, respectively (Weber, 1991).

The effect of radiation on leaching of radionuclides from glass is related to increasing surface area of their interaction with water due to microfissuring and to an increasing rate of glass dissolution. The latter is caused by changes in the chemical composition of glasses, their microstructure, and the nature of bonds between the framework elements. Irradiation from every source increases the rate of glass dissolution by two to four times. The rate increases almost proportionally to the increase in the sample area due to microfissuring. All these phenomena will be observed in HLW-bearing glasses after the first few hundred years of their storage.

EFFECT OF RADIATION ON CRYSTAL STRUCTURE

The effect of radiation on the properties of crystalline matrices is more significant. This is related to larger α irradiation doses being accumulated over the same time interval in crystalline matrices as compared to glasses (Table 1). Structural damage is accumulated progressively with increasing irradiation dose. The curve of amorphization as a function of irradiation dose is *S*-shaped (Ewing *et al.*, 1995). Therefore, the corresponding structural changes can be subdivided into three stages. At small irradiation doses, the structural damage is expressed in the existence of isolated defects (displacement cascades) a few nanometers in size (Figs. 1, 2). They form by collision of recoil nuclei with lattice atoms. At this stage, the reflexes on X-ray diffraction patterns are still intensive and electron diffraction shows dotty patterns. The amount of such defects (and the damaged volume) increases with increasing dose. Individual displacement cascades overlap, and domains with preserved ordered atom patterns are embedded in amorphous areas. Reflexes on X-ray dif-

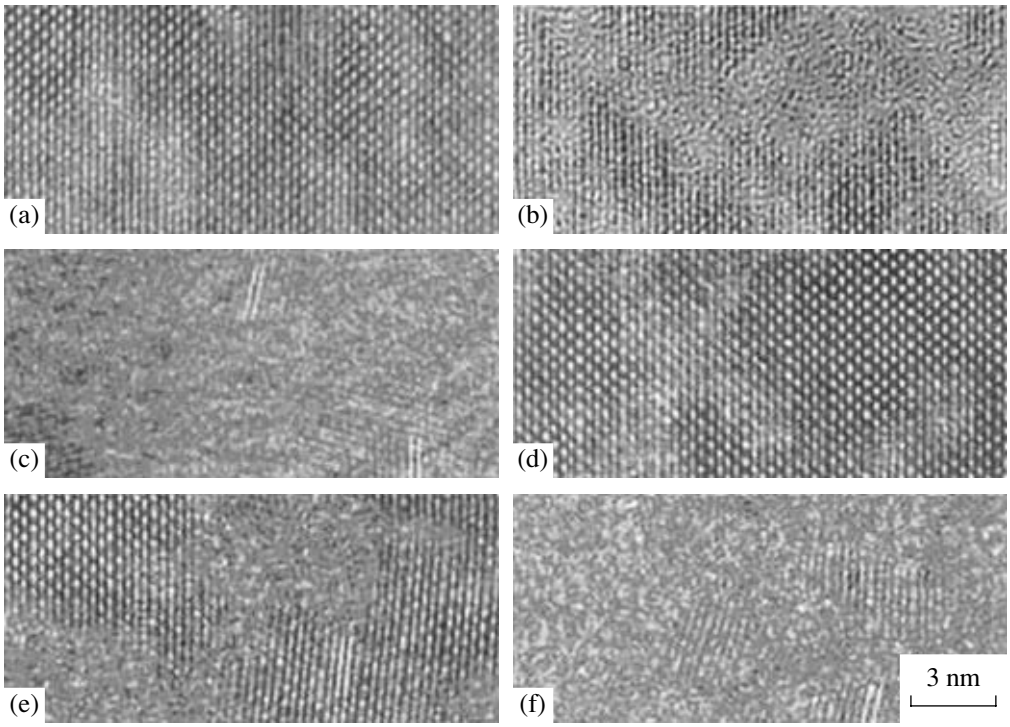

Fig. 2. Structural damage to natural zircon during α decay (a–c) and its synthetic analogue irradiated with 1.5 MeV Kr^+ ions (d–f) (Weber *et al.*, 1998). (a) 5×10^{16} α decay events/g (0.003 dpa); (b) 1.8×10^{18} α decay events/g (0.091 dpa); (c) 6.4×10^{18} α decay events/g (0.32 dpa); (d) 5×10^{13} Kr^+/cm^2 (0.057 dpa); (e) 1.5×10^{14} Kr^+/cm^2 (0.17 dpa); (f) 3×10^{14} Kr^+/cm^2 (0.34 dpa).

fraction patterns are modified into wide asymmetric peaks with low intensities, while reflexes on electron diffraction patterns become blurred and arc-shaped. At large irradiation doses, the material becomes X-ray amorphous, which corresponds to the final stage of radiation damage. The electron diffraction pattern shows a wide diffuse ring around the central reflex of the electron beam instead of the dotty reflexes observed at the first stage.

For zircon, first-stage damage is observed at irradiation doses $<3 \times 10^{18}$ α decay events/g; second-stage damage, at doses of $(3–8) \times 10^{18}$ α decay events/g; and complete amorphization (third-stage damage), at doses $>8 \times 10^{18}$ α decay events/g (Murakami *et al.*, 1991). Close values were obtained for natural zirconolite and pyrochlore, while perovskite requires larger doses for amorphization, $(3–6) \times 10^{19}$ α decay events/g (Lumpkin *et al.*, 1994, 1998_1, 2001). Some minerals (uraninite, monazite) preserve their structures even at very large doses (*Radioactive …*, 1988; Ewing *et al.*, 1995; Weber and Ewing, 2002). High resistance is related to a high restoration rate of radiation defects, exceeding the rate of defect formation.

METHODS FOR STUDYING RADIATION DAMAGE

Three approaches are usually used in analysis of radiation damage to matrix structure (Weber, 1991, Mamaev *et al.*, 1992; Ewing *et al.*, 1995; Weber *et al.*, 1986, 1998; Weber and Ewing, 2002). The first of them is based on study of natural radioactive (U,Th)-bearing minerals. In the second case, several weight percent of short-lived actinide isotopes, e.g., ^{238}Pu ($T_{1/2}$ = 88 yr) or ^{244}Cm ($T_{1/2}$ = 18 yr), are introduced into the structures of synthetic phases. In the third approach, a solid target is irradiated with neutral or charged particles (neutrons, electron, α particles, heavy ions). These approaches are compared in Tables 2 and 3.

Each approach possesses some advantages, but also has some limitations regarding use and data interpretation. Radiation damage is studied for many natural minerals with radioactive elements, e.g., zirconolite, pyrochlore, zircon, and perovskite. However, this method is not appropriate for many matrices. It cannot be applied for murataite-type phases or zirconium dioxide, because their natural analogues (murataite and tazheranite) do not contain radioactive elements. Moreover, some promising actinide matrices, such as REE zirconates with a pyrochlore structure and alumoferrites with a garnet structure, have no natural analogues. According to degree of similarity to HLW matrices, the natural minerals can be subdivided into three groups (Table 4). They are structural analogues of synthetic compounds proposed for actinide immobilization but can be similar (group 1) or dissimilar (group 3) to them in chemical composition. It is clear that the estimation of the radia-

Table 2. Comparison of interaction of various types of irradiation with the zirconolite crystal lattice (Lumpkin *et al*., 1996)

Irradiation mode	Energy, keV	Number of collisions with lattice atoms	Energy consumption for ionization, rel. %	Track, nm	Number of collisions per 1 nm track
α particle	4200	260	99	11000	≪1
^{232}Th	86	1400	45	24	58
^{238}U	72	1200	43	21	57
^{238}Pu	92	1490	45	24	62
^{244}Cm	96	1560	45	25	62
Kr^+	1000	540	84	>50	<11
Fast neutrons	0.05	570	53	46	12

Table 3. Approaches to analysis of radiation damage to an actinide matrix structure

Study of natural radioactive mineral analogues	Incorporation of actinides into structures of synthetic phases	Irradiation with accelerated heavy ions with high energies
	Advantages	
1. Wide interval of accumulated doses depending on mineral age and U and Th contents	1. Actinide-bearing phases with certain compositions and structures can be synthesized and studied	1. Short irradiation time (several minutes)
2. The processes are analogous to those operating in synthetic matrices	2. The processes are analogous to those operating in real actinide-bearing matrices	2. Induced activity is absent in materials
3. The radiation effect on matrix resistance (behavior) can be estimated in a real geological medium		3. The critical doses and their dependence on temperature can be estimated for every phase simultaneously
		4. Damage is observed during irradiation
		5. Any natural and synthetic materials can be studied
	Limitations	
1. Data are difficult to interpret because of the complex thermal history of minerals	1. Special equipment is needed because of high radioactivity	1. Different (external) mechanism of radiation impact
2. Natural analogues are nonradioactive (murataite, tazheranite) for some phases or are absent for others, e.g., (REE-Al,Fe) garnets and perovskites and (REE-Zr,Ti) pyrochlores	2. Long periods (years) are required for accumulation of needed irradiation doses	2. Damage zone is very thin
	3. Temperature dependence of the critical dose is difficult to determine	3. A special code is need for recalculating doses
		4. Critical doses and temperatures depend on the type of ions used for irradiation
		5. An accelerator of charged particles is needed

Table 4. Classification of synthetic phases used as actinide-bearing matrices by their similarity to natural minerals with analogous structures

1. There are mineral analogues, including radioactive ones	Zircon, zirconolite, pyrochlore, britholite, perovskite, brannerite, monazite, etc.
2. There are nonradioactive minerals of similar composition	Tazheranite (ZrO_2), kosnarite (NZP* phases), kimzeyite (Zr-bearing garnet), etc.
3. Natural minerals of similar chemical composition are absent	Murataite-type phases, REE zirconate with a pyrochlore structure, ferrites and aluminates with garnet and perovskite structures, etc.

* Sodium–zirconium phosphate with stoichiometry of $[NaZr_2(PO_4)_3]$.

tion stability of synthetic crystalline actinide matrices is less reliable for minerals of the third group than the first.

For study of the radiation damage in synthetic phases, their structures are doped with several weight percent of ^{238}Pu, ^{241}Am, or ^{244}Cm, with half-lives of 88, 433, and 18 yr, respectively. Up to 10^{20} α decay events occur in 1 g of such a matrix over several years of its storage. HLW ceramics will receive the same dose only after several hundred thousand years (Table 1). The processes operating during such experiments are analogous to those occurring during actinide decay in real HLW matrices. These experiments should be performed only in specially equipped laboratories ("hot" chambers) because of the high radioactivity of the materials studied.

These limitations are lacking in the method of irradiation of matrices with heavy ions of inert gases (Ne, Ar, Kr, and Xe), as well as with ions of Cs, Pb, Au, and so on. The irradiated material shows no induced activity, which simplifies its further study. The method is very rapid (irradiation lasts several minutes) and illustrative (the lattice destruction is observed *in situ* during irradiation with a transmission electron microscope). The radiation resistance and its temperature dependence can be determined during one session for all phases in the sample. Because of the short time of irradiation (hundreds of seconds), the intensity of damage induced by the radiation exceeds the rate of defect accumulation in matrices with real HLW by about 10^9 times. Special studies were needed to verify the correctness of application of data on ion irradiation in estimating the radiation resistance of matrices with real actinides.

Such verification was performed (Ewing *et al.*, 1995; Ewing, 1999) by comparing the damage to zirconolite and zircon structures caused by a ^{238}Pu admixture in synthetic phases, ^{238}U and ^{232}Th decay in natural minerals, and their irradiation with heavy ions. It was found that the accelrated irradiation induced lattice damage similar to that accumulated in natural minerals over a long time (Fig. 2). Thus, irradiation with heavy ions imitates well the interaction of lattice atoms and recoil nuclei resulting from actinide decay. The values of radiation resistance determined during heavy ion irradiation experiments and from decay of isomorphic actinides were found to be very similar. As a result, accelrated irradiation has been widely applied recently in study of radiation resistance of HLW matrices. We have used it for amorphization of phases with pyrochlore, zirconolite, murataite, brannerite, britholite, and garnet structures.

GROUNDS FOR SELECTING MATERIALS FOR THE STUDY

One of the conditions for selecting an HLW-confining matrix is a high capability of its structure to incorporate HLW components. This condition is met by phases with fluorite (pyrochlore, zirconolite, murataite), garnet, and apatite–britholite-type structures. There are several structural sites (two sites in the pyrochlore lattice and three or four sites in the murataite, garnet, britholite, and zirconolite lattices) that can be occupied by cations with various charges and sizes. This favors incorporation of various HLW components, including actinides, neutron absorbers, decay products, corrosion products, technological admixtures, and so on. Let us briefly review the main structural features of these compounds.

The pyrochlore, zirconolite, and murataite structures are derivatives of the fluorite structure with the general formula MO_2 (M = Zr, Hf, Tb, Ce, U, Th, etc.; a = 5.07–5.47 Å; space group $Fm3m$). The fluorite lattice consists of cubic polyhedra sharing common edges, like a 3D chessboard (Belov, 1950). Such a structure is typical of oxides of tetravalent actinides (Th, U, Np, and Pu), as well as CeO_2. Zirconium dioxide can crystallize in monoclinic, tetragonal, and cubic systems. Transition of the monoclinic modification to the tetragonal one occurs (according to various data) at 1050–1160°C, and the tetragonal structure transforms to the cubic one at temperatures above 2300°C. Admixture of Ca, REE, and actinide oxides shifts the field of stability of the cubic modification to lower temperatures. For example, with addition of 10–35 mol % Y_2O_3, the cubic variety form at 600°C (Maddrell, 1996). Incorporation of trivalent REE ions is accompanied by a decrease in the oxygen anion number and formation of vacancies. Phase compositions can be described by the following formula: $[(\mathrm{REE, An})_x^{3+}(\mathrm{An, Zr})_{1-x}^{4+}]O_{2-0.5x}$, An^{3+} = Pu, Am, Cm; An^{4+} = U, Np, Pu. Cation ordering between two structural sites with formation of a pyrochlore structure occurs at high concentrations of some elements, particularly light lanthanides.

The pyrochlore structure ($Fd3m$, Z = 8) can be represented as two fluorite cells sharing a common edge, with a half of the coordination polyhedra each lacking two diagonal anions (Belov, 1950). As a result, the cube is modified to a flattened octahedron and the formula is transformed from $^{VIII}A_4X_8$ (quadruple fluorite formula) into $^{VIII}A_2^{VI}B_2^{IV}Y_6^{IV}X$. A and B are cations in two structural sites. Y and X are anions; Y (O^{2-} anions) are involved in octahedra, while X (O^{2-}, F^-, Cl^-, OH^-) are located in interstices and do not participate in the structural framework. The coordination numbers (CN) of ions in this structure can be described by the following codes: AX_6Y_2, BX_6, XA_2B_2, and YA_4.

The zirconolite structure consists of nets of three- and six-member rings of Ti–O polyhedra. Three of four Ti atoms are surrounded by six oxygen atoms and one, by five oxygen atoms (Mazzi and Munno, 1983; Giere *et al.*, 1998). The interstices between nets of Ti–O polyhedra are occupied by Ca (CN = 8) and Zr (CN = 7) cations. Depending on the positional relationships between neighboring nets of Ti–O polyhedra, various structural modifications can occur, with monoclinic (zirconolite-

Table 5. Compositions of samples and phases in the titanate matrices, wt %

Sample	Phase	CaO	MnO	REE_2O_3	UO_2	ZrO_2	Al_2O_3	TiO_2	FeO	Other phases
IMM	WS	10.0	10.0	–	10.0	5.0	5.0	55.0	5.0	Rut, Cr, Gl
	M-5x	11.5	9.1	–	12.0	8.3	3.7	50.7	4.7	
	M-3x	9.4	11.9	–	5.3	3.0	9.3	52.8	8.3	
M17	WS	10.0	10.0	–	10.0	5.0	5.0	55.0	5.0	Rut
	M-5x	12.2	9.3	–	9.7	5.8	4.4	51.1	4.5	
	M-8x	10.9	12.2	–	8.1	2.8	6.1	53.2	6.7	
M3/7 (REE = Ce)	WS	8.0	8.0	20.0	8.0	4.0	4.0	44.0	4.0	Cr
	Pyr	8.9	5.1	27.7	10.5	4.5	0.9	39.6	1.0	
	M-8x	8.7	10.9	11.5	2.8	1.6	7.9	49.4	7.2	
Z24 (REE = Gd)	WS	6.0	–	32.0	–	25.0	9.0	28.0	–	Rut, CO, Gl
	Zir	4.4	–	35.1	–	10.5	7.9	41.8	–	
F3	WS	10.0	–	–	47.0	2.0	1.0	40.0	–	Rut, CO
	Pyr	16.1	–	–	46.2	3.3	0.3	34.1	–	
	Br	3.6	–	–	51.2	2.7	0.7	41.9	–	

Note: WS, whole sample; Zir, zirconolite; Pyr, pyrochlore; Br, brannerite; M-3x, M-5x, and M-8x, murataites with three-, five-, and eightfold fluorite-type unit cells; Rut, rutile; Cr, crichtonite; Gl, glass; CO, oxide with a fluorite structure.

2M), orthorhombic (zirconolite-3O), or trigonal (zirconolite-3T) symmetries (Bayliss *et al.*, 1989).

The structure of natural murataite with general formula $A_6B_{12}C_4TX_{40-x}$ (A = Y, Na; B = Ti; C = Fe; T = Zn; X = O, F) is determined as cubic, $F\bar{4}3m$, a = 14.89 Å, Z = 4 (Ercit and Hawthorne, 1995). The structure has four sites for cations: $A^{[8]}$ is a distorted cube with eightfold coordination, $B^{[6]}$ is an octahedron, $C^{[5]}$ is a fivefold-coordinated polyhedron (trigonal bipyramid), and $T^{[4]}$ is a regular tetrahedron. Octahedra share edges in B_3X_{13} groups, four of which, sharing vertices, form a tetrahedron-shaped polyanion known as the Keggin structure $[B_{12}TX_{40}]^{n-}$ with a tetrahedral vacancy T in its center and a $C^{[5]}$ polyhedron within the hexagonal faces of the tetrahedron. A synthetic murataite-type phase with formula $[(Ca,Mn)_2Zr(Fe,Al)_4Ti_3O_{16}]$ was discovered in ceramics developed for immobilization of radioactive wastes of the Savannah River plant in the United States (Morgan and Ryerson, 1982). Its structure can be expressed by the oxide fluorite-type motif with a threefold unit cell parameter. Murataite phases with five- and eightfold fluorite unit cell parameters were found in matrices for HLW immobilization at the Mayak radiochemical plant (Laverov *et al.*, 1998_1). Mössbauer spectroscopy shows that Fe(III) in both varieties is distributed between B octahedral and C [5]-coordinated polyhedra in a proportion of 3 : 1, while the tetrahedral sites are vacant (Urusov *et al.*, 2002). Thus, the refined formula of synthetic murataite can be written as $A_3^{[8]}B_6^{[6]}C_2^{[5]}O_{22-x/2}$.

The apatite–britholite structure (Aleksandrova *et al.*, 1966) consists of polyhedra with a central cation of Ca (or REE) bonded through $(PO_4)^{3-}$ or $(SiO_4)^{4-}$ groups. There are two types of structural polyhedra, [9]- and [7]-coordinated. The [9]-coordinated sites are occupied by 1/3 of the Ca ions, while 2/3 of the Ca ions are surrounded by six O^{2-} anions and one F^-, Cl^-, or OH^- anion. The mineral formula is (Ito, 1968) $^{IX\text{-}VII}A_{10}^{IV}B_6O_{24}X_2$ ($P6_3/m$, Z = 1); A = Ca, REE, Th, Al, Fe, Mn, Mg, Na, K; B = Si, P, B, F, Al; X = O, OH, F. Britholite can be considered as an apatite variety with the substitution Ca + P ⟶ REE + Si.

The garnet structure is typical of phases with formula $^{VIII}A_3^{VI}B_2{}^{IV}X_3O_{12}$ ($Ia3d$, Z = 8) and is a trimeric framework of alternating XO_4 tetrahedra and BO_6 octahedra sharing common vertices (Geller, 1967). The interstices, distorted cubes in shape, are occupied by the largest cations. The existence of three sites with CN = 8, 6, and 4 allows potential incorporation of various elements into the garnet structure. The $[A]^{VIII}$ site normally includes divalent (Ca, Mn, Mg, Fe, Co, Cd), trivalent (Y, REE, An), and tetravalent (An) cations (An = Th, U, Pu, Np, Am). Trivalent (Fe, Al, Ga, Cr, Mn, In, Sc, V) and tetravalent (Zr, Ti, Sn) cations occupy the $[B]^{VI}$ site. The $[X]^{IV}$ site is filled with trivalent (Al, Ga, Fe), tetravalent (Ge, Si, Ti), and pentavalent (V, As) cations.

SAMPLE DESCRIPTION

The radiation resistance was studied for 11 samples of titanate, silicate, and ferrite matrices (Tables 5, 6). The HLW components are incorporated into oxides with fluorite-type structures (zirconolite, pyrochlore,

Table 6. Compositions of samples and phases in the ferrite and silicate matrices, wt %

Sample	Phase	CaO	REE_2O_3	UO_2	ZrO_2	Al_2O_3	SiO_2	Fe_2O_3	Other phases
G2 (REE = Gd)	WS	9.3	26.0	10.1	11.8	22.0	–	20.8	Ur, Hib
	Gar	10.6	34.8	2.7	21.2	10.3	–	20.4	
G3 (REE = Gd)	WS	8.6	15.9	15.8	13.5	7.6	–	38.6	Ur, Hib
	Gar	10.5	32.6	2.6	22.8	7.3	–	24.2	
G4	WS	12.9	–	15.4	42.3	7.8	–	21.6	CO, Hib
	Gar	21.4	–	15.8	29.5	8.5	–	24.8	
G56 (REE = Gd, Ce)	WS	27.1	18.0	–	–	–	29.1	25.8	Br, Wo, Mag
	Gar	25.2	14.7	–	–	–	25.3	34.8	
G77 (REE = Nd, Ce, La, Eu)	WS	29.3	18.0	–	5.9	–	31.4	15.4	Br, Wo, Gl
	Gar	25.5	8.5	–	10.0	–	24.1	31.9	
G88 (REE = Nd, Ce, La, Eu)	WS	24.7	21.9	–	7.4	–	37.1	8.9	Gar, Wo
	Br	15.2	54.2	–	6.7	–	23.1	0.8	

Note: WS, whole sample; Gar, garnet; Br, britholite; Ur, Ca uranate; CO, oxide with a fluorite structure; Hib, hibonite; Wo, wollastonite; Mag, magnetite; Gl, glass.

muratatite), uranium titanate (brannerite), and ferrites and silicates with garnet-type structures, as well as (Ca, REE) silicate with an apatite-type structure (britholite). The titanate ceramics are synthesized by inductive melting in a cold crucible (samples IMM, Z24, and F3) or by melting in a resistance furnace (samples M17 and M37) at temperatures of 1550–1600°C. Silicate matrices (samples G56, G77, and G88) are synthesized by inductive melting in a cold crucible. Ferrites with garnet-type structures (samples G2, G3, and G4) are obtained by pressing followed by sintering at 1400°C. Before irradiation, the samples were studied by X-ray powder diffraction (DRON-3, Cu irradiation); scanning electron microscopy (JSM5300 with EDS LINK ISIS);

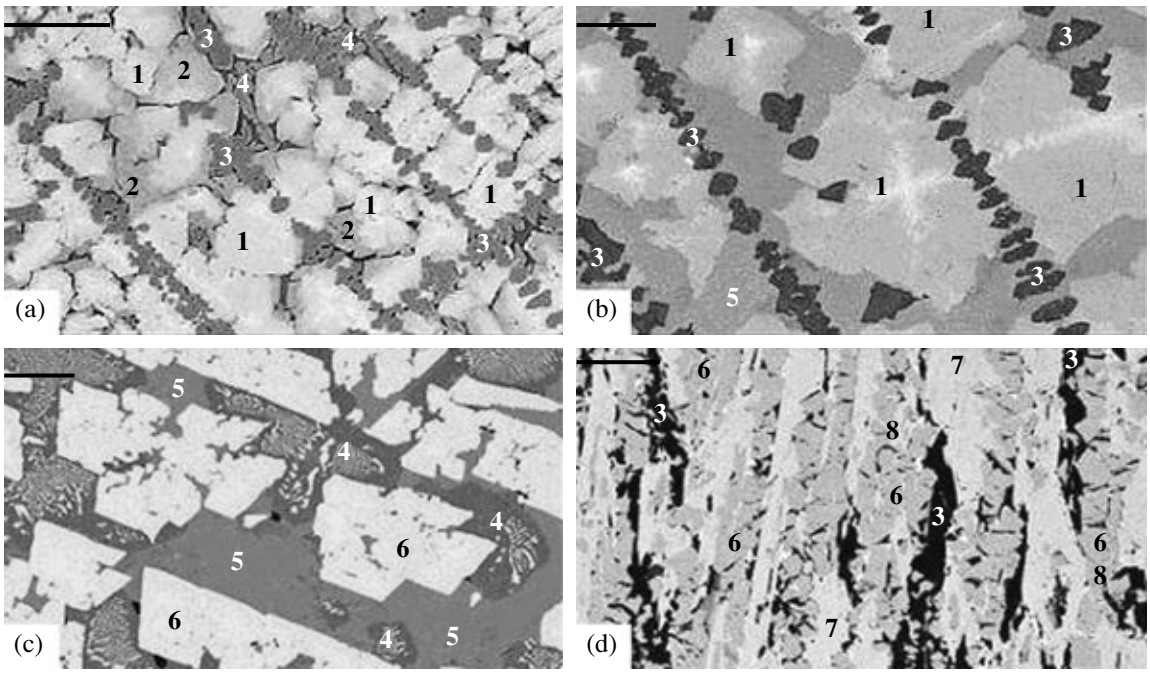

Fig. 3. BSE images of muratatite (a–c) and pyrochlore (c, d) matrices: (a) sample IMM, (b) sample M17, (c) sample M37, and (d) sample F3. (1) Muratatite-5x; (2) muratatite-3x; (3) rutile; (4) crichtonite; (5) muratatite-8x; (6) pyrochlore; (7) brannerite; (8) cubic U dioxide (small white inclusions). The bar is equal to 50 μm.

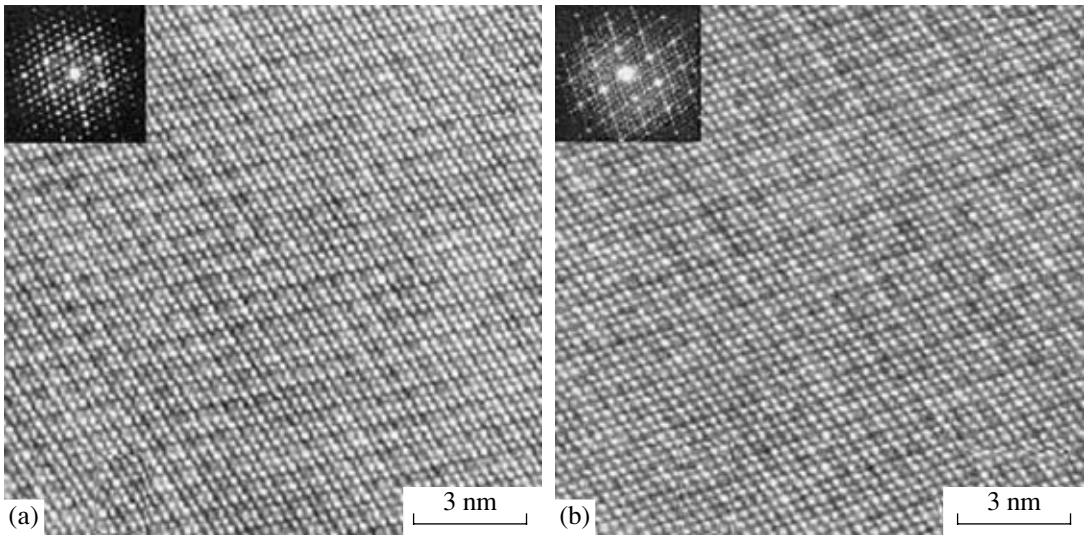

Fig. 4. TEM and high-resolution TEM images of the [1–10] plane of murataite-3x (a) and murataite-5x (b) in sample IMM.

and transmission electron microscopy (JEM-100c), including high-resolution TEM (JEM-4000EX). Synthesis conditions and data on the sample composition are considered in (Stefanovsky *et al.*, 2001_1; Stefanovsky *et al.*, 1999, 2001_2; Yudintsev, 2001; Yudintsev *et al.*, 1999, 2001; Smelova *et al.*, 2000; Urusov *et al.*, 2002; Lian *et al.*, $2002_{1,2}$; Utsunomiya *et al.*, $2002_{1,2}$). Some results of previous studies are briefly reviewed below.

TITANATE MATRICES WITH PHASES WITH FLUORITE-TYPE STRUCTURES

Sample IMM consists of murataite and minor rutile, crichtonite, and glass. Murataite is represented by varieties with three-, five- and eightfold fluorite motifs with dominant murataite-5x (Figs. 3, 4). The mineral typically has a zonal structure. U and Zr concentrations decrease and Fe and Al contents increase toward the grain margins. The mineral formulas are as follows: $[(Ca_{1.35}U_{0.17}Zr_{0.17}Mn_{1.35}Ti_{5.5}Fe_{0.94}Al_{1.52})O_{18.1}]$ in the margins of a grain and $[(Ca_{1.87}U_{0.42}Zr_{0.5}Mn_{1.1}Ti_{5.85}Fe_{0.59}Al_{0.67})O_{18.5}]$ in its core. Rutile and crichtonite compositions are stoichiometric: $[(Ti_{0.95}Zr_{0.03})O_{1.96}]$ and $[(Ca_{0.1.5}U_{0.1}Zr_{0.1}Mn_{2.3}Ti_{13.9}Fe_{1.9}Al_{2.0})O_{38.0}]$. The glass composition is as follows (wt %): 3.7 Na_2O, 16.1 Al_2O_3, 32.0 SiO_2, 18.4 CaO, 11.9 TiO_2, 10.6 MnO, and 2.1 Fe_2O_3, with ZrO_2 and UO_2 contents below the detection limit (0.3 wt %). The glass formation is related to dissolution of the crucible liner in the melt during the experiment.

Sample M17 consists of murataites with five- and eightfold fluorite unit cells and rutile (Figs. 3, 5). The Ca, U, and Zr contents decrease and the Mn, Ti, Fe, and Al contents increase in murataite-5x from cores of grains to their margins. The corresponding formulas are $[(Ca_{2.28}U_{0.42}Zr_{0.76}Mn_{1.0}Ti_{5.69}Fe_{0.42}Al_{0.42})O_{18.3}]$ and $[(Ca_{1.94}U_{0.33}Zr_{0.56}Mn_{1.18}Ti_{5.74}Fe_{0.5}Al_{0.85})O_{18.3}]$. Murataite-8x and rutile are more homogeneous, having the respective formulas $[(Ca_{1.65}U_{0.25}Zr_{0.19}Mn_{1.46}Ti_{5.65}Fe_{0.79}Al_{1.01})O_{17.6}]$ and $[(Ti_{0.91}Zr_{0.03})O_{1.88}]$. The margins of the murataite-5x grains are close in composition to murataite-8x.

Sample M37 consists of pyrochlore, murataite-8x, and crichtonite with the respective formulas $[(Ca_{0.6}Mn_{0.3}Ce_{0.7}Zr_{0.2}U_{0.2}Ti_2Al_{0.1})O_7]$, $[(Ca_{1.33}Ce_{0.6}Zr_{0.11}U_{0.09}Mn_{1.32}Ti_{5.33}Fe_{0.87}Al_{1.34})O_{17.51}]$, and $[(Ca_{0.8}Ce_{0.8}Zr_{0.4}Mn_2Ti_{12.2}Fe_{1.9}Al_{3.9})O_{38}]$. Murataite is represented by the variety with the eightfold fluorite motif (Fig. 6). The dominant U-bearing phase in this sample is pyrochlore (Fig. 3), unlike the ceramics mentioned above.

Sample F3 consists of pyrochlore, brannerite, rutile, and small grains of uranium oxide with a fluorite-type structure (Figs. 3, 7). The corresponding phase formulas are $[(Ca_{1.2}U_{0.8}Zr_{0.1}Ti_{1.9})O_{6.7}]$ (pyrochlore) and $[(Ca_{0.3}U_{0.7}Zr_{0.1}Ti_2Al_{0.1})O_6]$ (brannerite); the rutile formula is close to TiO_2.

Element proportions in sample Z24 correspond to Gd-bearing zirconolite. In addition to zirconolite, the sample contains Zr dioxide, pyrochlore, rutile, and glass (Figs. 3, 8, 9). The zirconolite formula is close to $[(Ca_{0.4}Gd_{0.8}ZrTi_{1.4}Al_{0.4})O]$. Small Zr dioxide grains are located within the zirconolite crystals, while glass fills the interstices among zirconolite grains and includes rutile crystals. The glass contains almost all silica, which is derived by partial dissolution of the crucible liner. The glass composition is as follows (wt %): 1.2 Na_2O, 24.0 Al_2O_3, 40.9 SiO_2, 14.0 CaO, 8.3 TiO_2, and 12.6 Gd_2O_3, with Fe_2O_3 and ZrO_2 contents of <0.3 wt %.

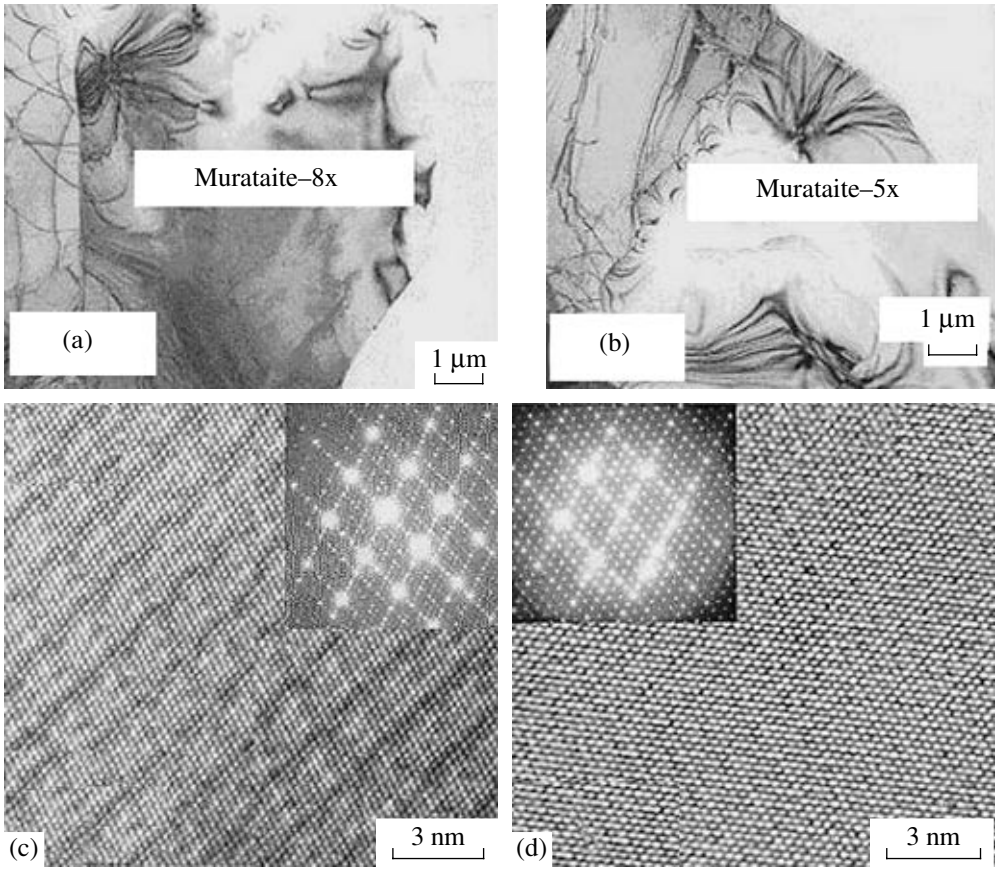

Fig. 5. Bright-field TEM images of murataite-type phases in sample M17 (a, b) and high-resolution TEM images of the [$\bar{1}$10] plane of murataite-8x (c) and murataite-5x (d).

FERRITE AND ALUMOFERRITE MATRICES WITH GARNET-TYPE STRUCTURES

Samples G2 and G3 consist of the following phases (ranged in decreasing proportion): garnet, Ca uranate, and Ca alumoferrite with a hibonite structure (Fig. 10). Zirconium dioxide is the major phase in sample G4, while garnet and hibonite occur in smaller amounts. The compositions of the irradiated phases are listed in Table 6. The formulas of phases with garnet structures are as follows: $[(Ca_{1.5}Gd_{1.5}U_{0.1}Zr_{1.4}Al_{1.6}Fe_{1.9})O_{12}]$ (sample G2), $[(Ca_{1.5}Gd_{1.5}U_{0.1}Zr_{1.5}Al_{1.1}Fe_{2.3})O_{12}]$ (sample G3), and $[(Ca_{2.7}U_{0.3}Zr_{1.7}Al_{1.1}Fe_{2.2})O_{12}]$ (sample G4). The formulas were calculated with the assumption that iron is trivalent and uranium is tetravalent.

SILICATE PHASES WITH GARNET AND APATITE–BRITHOLITE STRUCTURES

The samples contain silica in amounts increasing from sample G56 to sample G88 (Table 6). Simultaneously, the proportion of garnet decreases, while the proportions of (Ca, REE) silicate with an apatite structure (britholite) and Ca silicate (wollastonite) increase (Fig. 11). Minor magnetite (sample G56) and glass (sample G77) are also found. The formulas of major phases are as follows: garnet, $[(Ca_{2.8}Ce_{0.16}Gd_{0.28}Fe_{2.48}Si_{2.4})O_{12}]$ (sample G56) and $[(Ca_{2.6}La_{0.02}Ce_{0.05}Nd_{0.15}Eu_{0.07}Zr_{0.46}Fe_{2.29}Si_{2.3})O_{12}]$ (sample G77); britholite, $[(Ca_{4.11}La_{0.79}Ce_{1.42}Nd_{2.22}Eu_{0.48}Zr_{0.79}Fe_{0.16}Si_{5.85})O_{25}]$ (sample G88). In the formula calculation, iron and lanthanides were taken to be trivalent. Actually, iron could be partially bivalent, and Ce, tetravalent. This could cause the deviation of total cation amounts in the formulas from the theoretical values of 8.0 for garnet and 16.0 for britholite.

STUDY OF RADIATION DAMAGE TO CERAMICS

The samples were irradiated with Kr and Xe ions with energies of 1.0 and 1.5 MeV in an accelerator at Argonne National Laboratory (United States). The experiments were performed at temperatures from 50 to 1053 K and a dose rate of 10^{11}–10^{12} ions/cm^2 s. The ion penetration depth into the solid target was several microns. Particles <1 μm thick with the highest grade of radiation damage were selected for structural analysis. Changes in electron diffraction patterns with

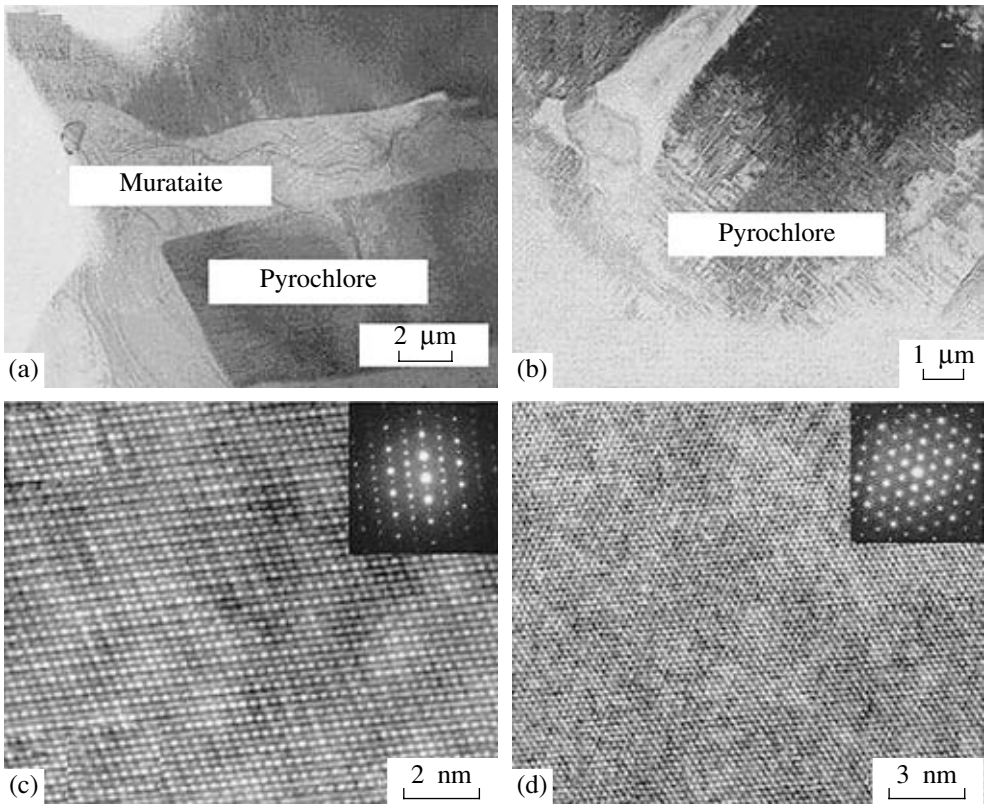

Fig. 6. Bright-field TEM images of sample M37 (a, b) and high-resolution TEM images of the [$\bar{1}$10] plane of pyrochlore (c) and the [11–1] plane of murataite-8x (d).

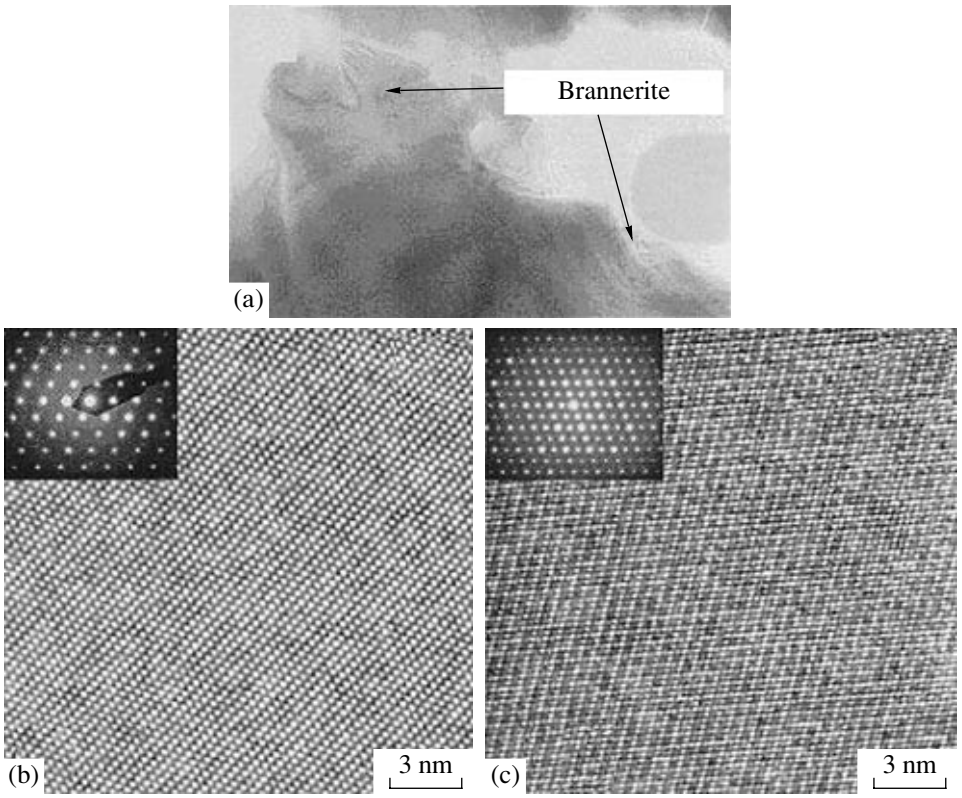

Fig. 7. Bright-field TEM image of sample F3 (a) and high-resolution TEM images of the [001] plane of brannerite (b) and the [110] plane of pyrochlore (c).

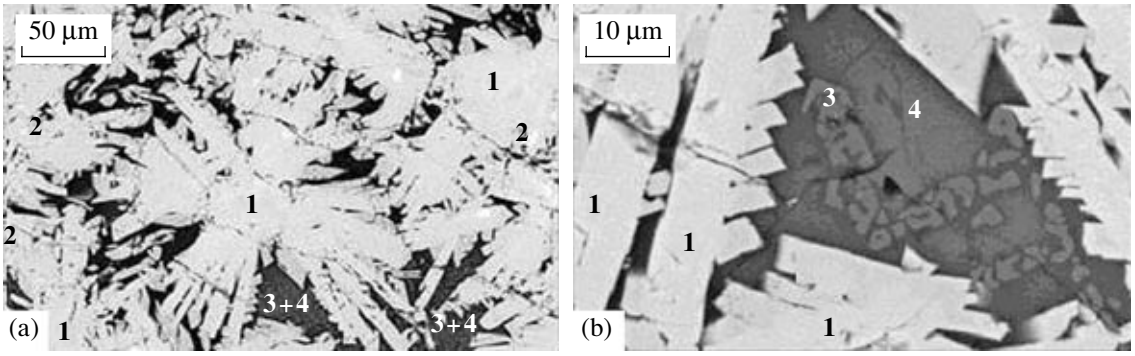

Fig. 8. BSE images of zirconolite matrix Z24: (a) general view; (b) a detail. (1) Zirconolite; (2) ZrO_2; (3) rutile; (4) glass.

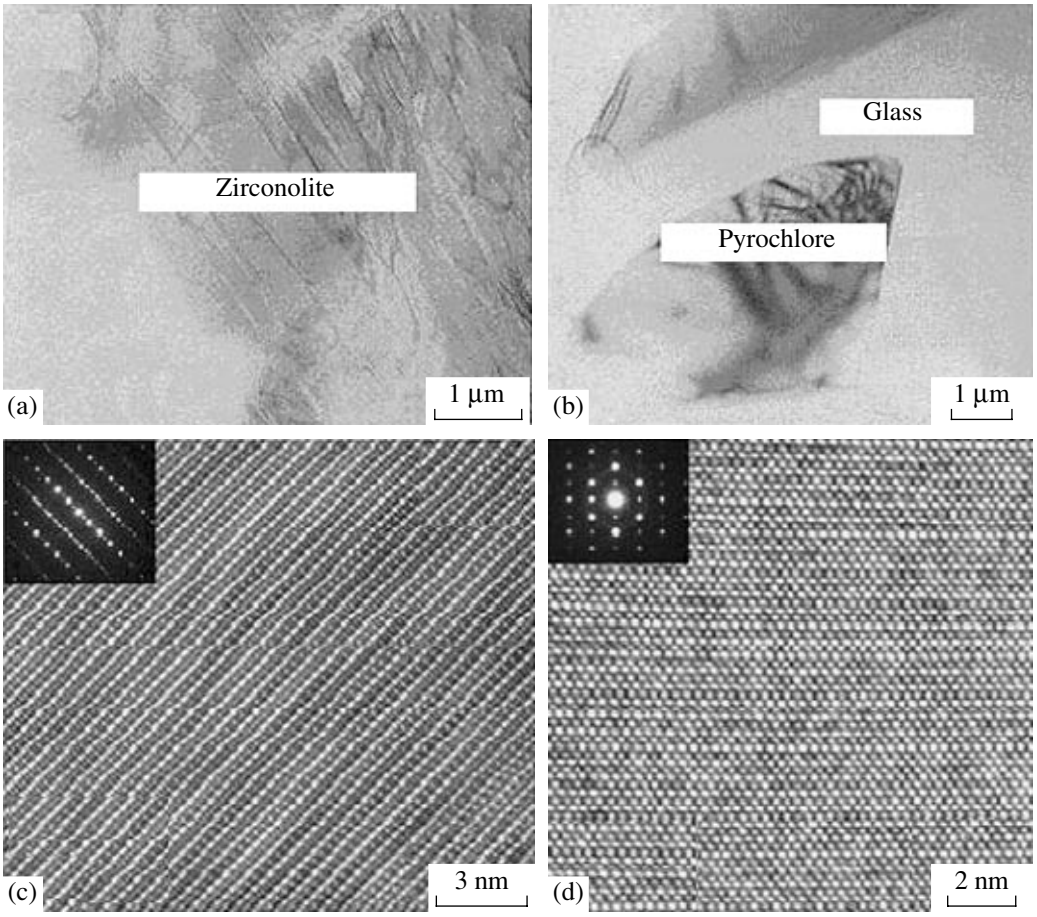

Fig. 9. Bright-field TEM images of sample Z24 (a, b) and high-resolution TEM images of the [–130] and [–110] planes (c, d).

increasing irradiation dose were observed with transmission electron microscopy (Figs. 12–14). The electron diffraction for samples before irradiation shows dotty patterns indicative of the high ordering of atoms in crystal structures. The irradiation disturbs the ordering, which leads to blurring of reflexes in the electron diffraction patterns and, finally, to replacement of the dotty pattern by a wide diffuse ring around the central reflex. The critical doses (D_{cr}) needed for complete structural amorphization were determined during irradiation *in situ* according to the transformation of the dotty diffraction pattern into the ring-shaped pattern. Amorphization in the irradiated phases can be seen under a high-resolution transmission electron microscope. The images show damage zones (tracks) formed by ion collision with lattice atoms (Figs. 15, 16).

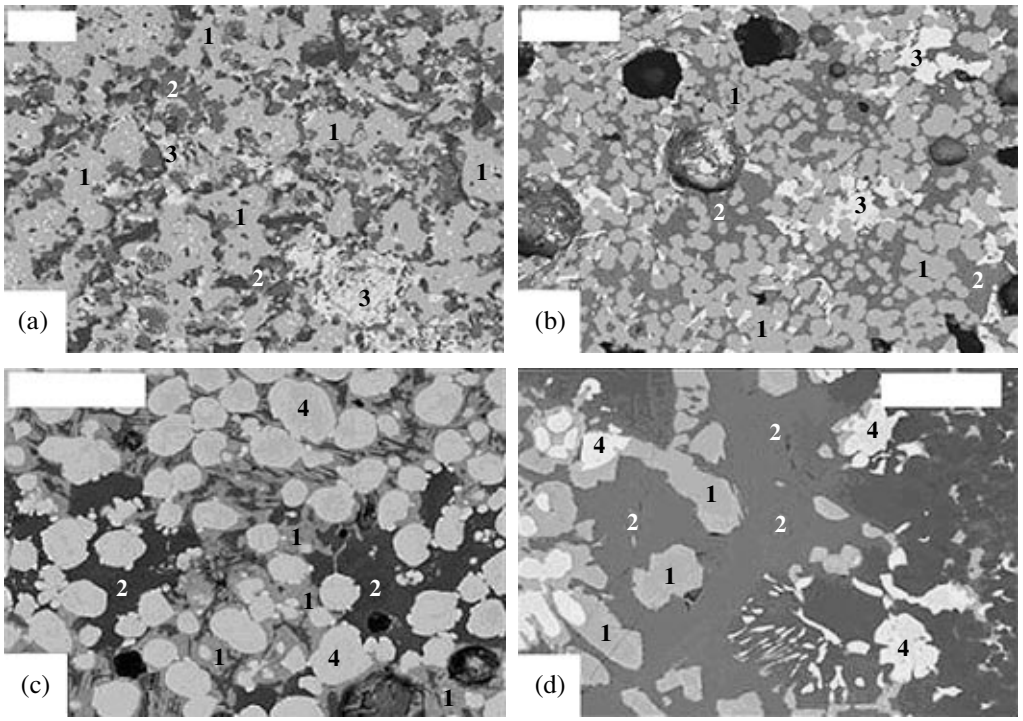

Fig. 10. BSE images of ferrite matrices G2 (a), G3 (b), and G4 [sample core (c) and sample margin (d)]. (1) Garnet; (2) hibonite; (3) Ca uranate; (4) ZrO_2. Black patches are pores. The bar is equal to 50 μm.

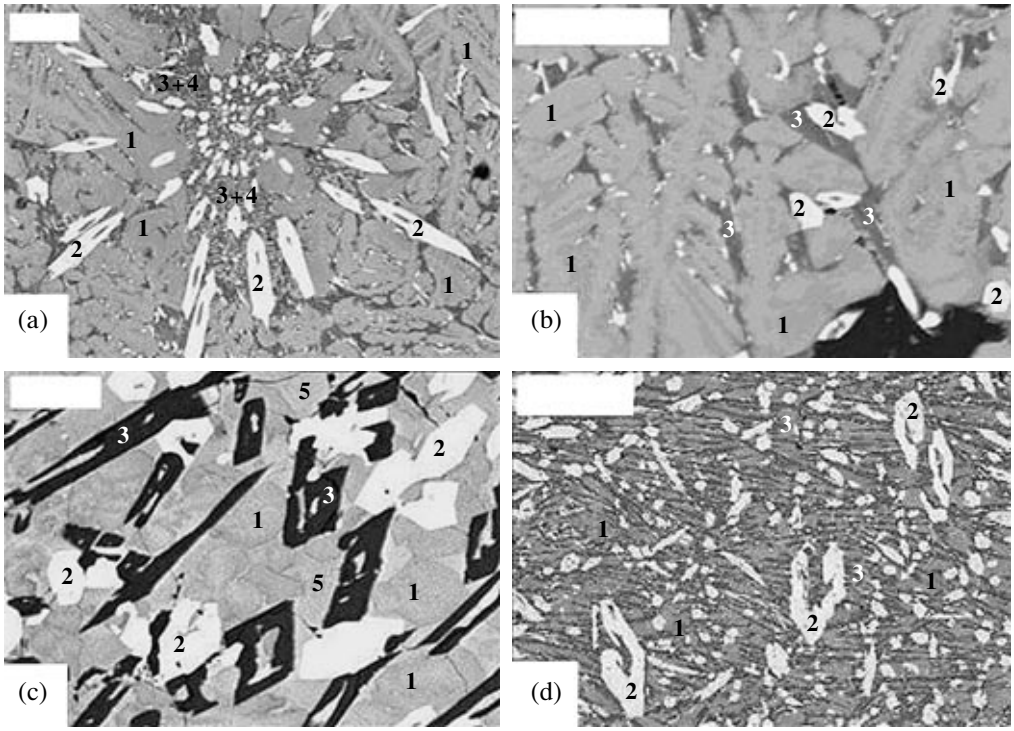

Fig. 11. BSE images of iron–silicate matrices G56 (a, b), G77 (c), and G88 (d). (1) Garnet; (2) britholite; (3) wollastonite; (4) magnetite; (5) glass. Black patches are pores. Bars are equal to 50 μm (a–c) and 150 μm (d).

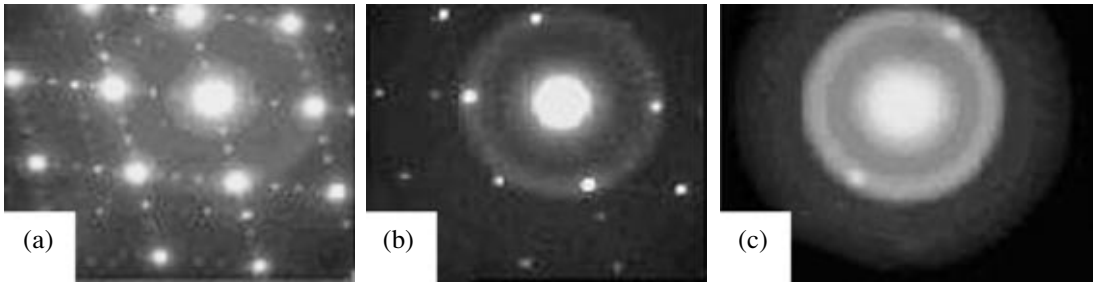

Fig. 12. TEM images of murataite-5x irradiated by Kr^+ ions: (a) 4.38×10^{13} ions/cm^2; (b) 9.39×10^{13} ions/cm^2; (c) 1.56×10^{14} ions/cm^2. Sample M17.

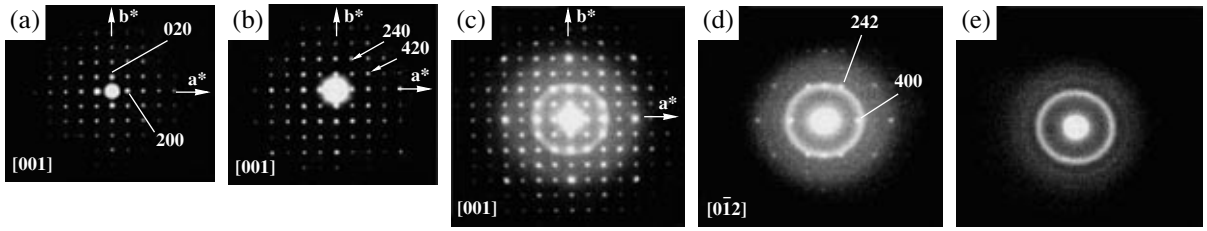

Fig. 13. Electron diffraction patterns of garnet (sample G3) before irradiation (a) and (b–e) irradiated with 1 MeV Kr^{2+} ions up to doses of (b) 0.09 dpa, (c) 0.14 dpa, (d) 0.18 dpa, and (e) 0.22 dpa.

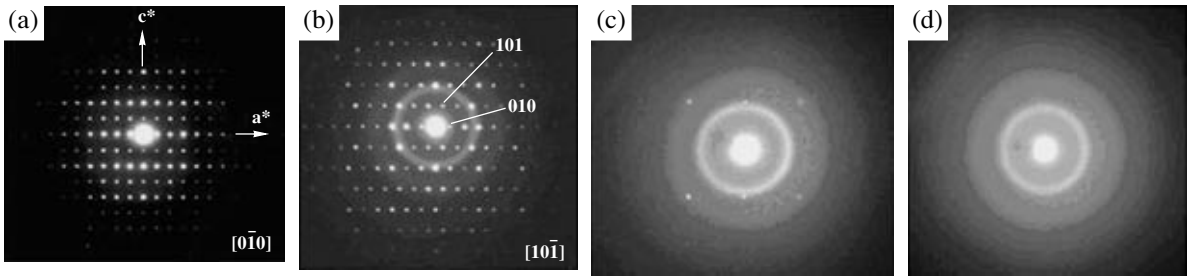

Fig. 14. Electron diffraction patterns of britholite (sample G88) before irradiation (a) and (b–d) irradiated with 1.5 MeV Xe^+ ions up to doses of (b) 0.19×10^{14} ions/cm^2, (c) 0.25×10^{14} ions/cm^2, and (d) 0.38×10^{14} ions/cm^2.

Structural restoration occurs together with the structural damage. At some critical temperature (T_{cr}), the restoration rate becomes higher than the rate of formation of new radiation defects. In this case, the crystal lattice does not change at any irradiation doses. The radiation resistance can be characterized by the values of the critical dose and critical temperature. The phases more resistant to radiation have higher D_{cr} and lower T_{cr} (Weber and Ewing, 2002).

Critical doses (doses for complete amorphization) were determined for all phases, and critical temperatures, for some of them (murataite and garnet) (Tables 7, 8; Fig. 17). Figures 12 and 15 demonstrate stages of progressive damage to the murataite structure with increasing dose. Disordering begins with disappearance of the murataite superstructure with preservation of the dotty electron diffraction pattern corresponding to the fluorite lattice. Further irradiation leads to complete amorphization of the phase structure, with the appearance of broad rings in the electron diffraction patterns and a chaotic distribution of atoms seen in the high-resolution TEM images. A similar phenomenon was earlier established for pyrochlore (Wang *et al.*, 1999_2). On irradiation, the initial lattice was primarily transformed into the intermediate structure of fluorite; then, with increasing dose, the phase was completely amorphized.

The radiation resistance of murataite increases in the sequence murataite-8x < murataite-5x < murataite-3x, with a decrease in the repetition factor of the fluorite unit cell. The transformation of pyrochlore, as a derivative of fluorite structure with a twofold fluorite unit cell parameter, also obeys this regularity. In sample M37, the pyrochlore-type phase is more stable than murataite (Table 7). The D_{cr} value for murataite is almost independent of temperature up to 800 K and is (1.6–1.9) $\times$ 10^{14} Kr^+/cm^2. The critical temperatures

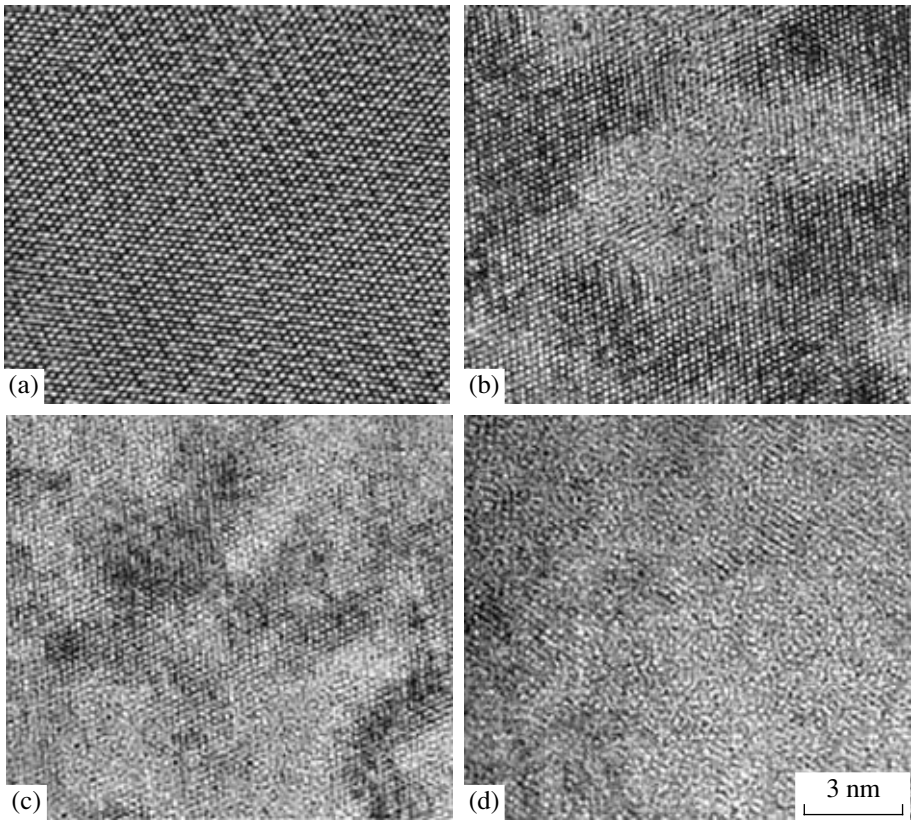

Fig. 15. High-resolution TEM images of murataite-5x (sample M17) before irradiation (a) and (b–d) irradiated with 1 MeV Kr^+ ions up to doses of (b) 4.38×10^{13} ions/cm^2, (c) 9.39×10^{13} ions/cm^2, and (d) 1.56×10^{14} ions/cm^2.

above which the phases in sample M17 are stable at any irradiation doses are 930 K for murataite-5x and 1030 K for murataite-8x.

Zirconolite has the highest resistance to radiation among the phases studied. A series of structural transformations of the initial zirconolite occurs on irradiation. The initial structure changes first to a pyrochlore structure and then to a cation-disordered fluorite-type lattice, finally being completely amorphized. The critical dose is ~3×10^{14} Kr^+/cm^2, which is close to values for zirconolites ($CaZrTi_2O_7$), ($CaZrNbFeO_7$), and ($Ca_{0.5}Nd_{0.5}ZrTi_{1.5}Al_{0.5}O_7$) (Wang *et al.*, 2000_1) and varieties with 0.1–0.2 formula units of U and Th (Smith *et al.*, 1998). Thus, the change in the molecular weight of zirconolite on substitution of REE and actinides for Ca and Al, Nb, and Fe for Ti does not significantly affect the resistance of the zirconolite structure to ion irradiation at room temperature.

Sample F3 contains, in addition to pyrochlore, U titanate with a brannerite structure (Figs. 3, 7; Table 5). A knowledge of the behavior of brannerite and its synthetic analogues on irradiation is important, because this phase occurs in many titanate matrices for actinide wastes. Actinides in these matrices are generally incorporated into pyrochlore and/or zirconolite, and the proportion of brannerite can reach 10–30 vol % (Ebbinghaus *et al.*, 1998; Yudintsev *et al.*, 1999; Burakov and Anderson, 2000; Stefanovsky *et al.*, 2001). Pyrochlore is more resistant to radiation than brannerite, for which $D_{cr} = 1.4 \times 10^{14}$ ions/cm^2 (Table 7). This could be related to the structural features of these phases. The pyrochlore structure consists of TiO_6 octahedra sharing

Table 7. Critical doses of ion irradiation (D_{cr}) for phases with a murataite structure, pyrochlore, zirconolite, and brannerite

Sample	IMM		M17		M37		Z24	F3	
Phase	M-5x	M-3x	M-8x	M-5x	Pyr	M-8x	Zir	Pyr	Br
D_{cr}, 10^{14} ions/cm^2	1.66 ± 0.06	1.85 ± 0.06	1.82 ± 0.06	1.85 ± 0.06	1.75 ± 0.13	1.69 ± 0.13	2.94 ± 0.06	2.36 ± 0.13	1.38 ± 0.06
D_{cr}, dpa	0.12	0.15	0.14	0.15	0.19	0.15	0.3	0.3	0.1

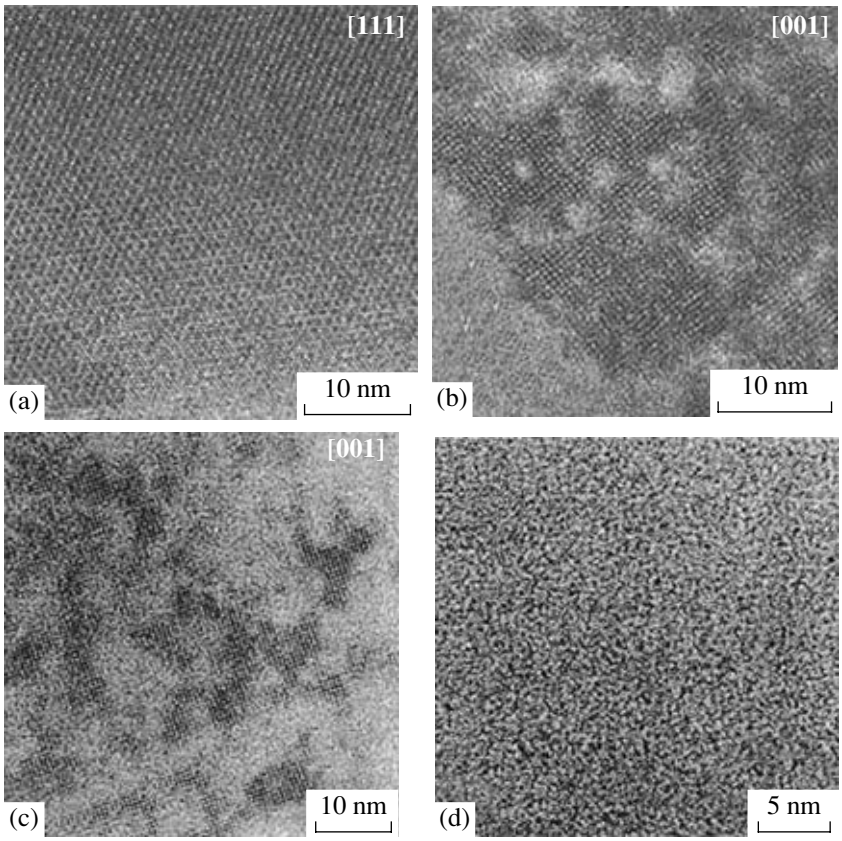

Fig. 16. High-resolution TEM images of garnet (sample G3) before irradiation (a) and (b–d) irradiated with 1 MeV Kr^{2+} ions up to doses of (b) 0.09 dpa, (c) 0.14 dpa, and (d) 0.22 dpa.

vertices to form a trimetric framework. It has a higher degree of linkage than the brannerite structure, where zigzag bands of TiO_6 octahedra share edges with polyhedra with U and Ca cations occupying the interstitial space. Because of this, the brannerite lattice can be amorphized at smaller irradiation doses than the pyrochlore lattice. The study of natural brannerite has shown its rather low radiation and chemical resistance.

Table 8. Critical doses of ion irradiation (D_{cr}) for phases with garnet and britholite structures at various temperatures

T, K	G2 (Gar)	G3 (Gar)	G4 (Gar)	G56 (Gar)	G77 (Gar)	G88 (Br)
	D_{cr}, 10^{14} ions/cm^2					
50	–	1.59	–	–	–	–
298	1.44	1.50	1.63	1.56	1.56	0.38*
373	–	1.53	–	–	–	–
573	–	1.73	1.88	–	–	–
673	–	–	1.63	–	–	–
773	–	1.81	3.75	2.00	–	–
823	2.19	–	–	2.13	–	–
873	2.25	–	15.8	2.56	3.19	–
923	2.81	2.59	–	–	–	–
973	–	–	–	3.50	7.06	–
1013	3.44	5.00	–	–	–	–
1053	3.44	52.5	–	6.88	–	–

* Britholite was irradiated with 1.5 MeV Xe^+ ions.

Up to 75–90% of primary uranium can be removed during brannerite alteration and replacement by secondary Ti hydroxides (Lumpkin *et al.*, 2000). Thus, the formation of titanates with a brannerite structure could decrease the capability of the matrix for confining actinides.

The D_{cr} values of britholite are lower than those of the other phases (Table 8), because britholite was irradiated by heavier ions of Xe^+ with an energy of 1.5 MeV. Similar differences in critical doses were determined for pyrochlore-type phases irradiated by ions with different masses (Ewing *et al.*, 1995).

The radiation resistance of ferrites and silicates with a garnet lattice is $1.4–1.6 \times 10^{14}$ ions/cm^2 at room temperature (Table 8). It is independent of the garnet composition (silica, REE, U, and Zr contents) up to a temperature of 700 K (Fig. 17). This behavior distinguishes the garnet structure from the pyrochlore one. The radiation resistance (critical dose) of pyrochlore increases with increasing Zr content (Wang *et al.*, 1999_1). Above 800 K, the critical dose for the garnet lattice increases. Depending on the composition, T_{cr} of garnet varies within the range 900–1100 K (Utsunomiya *et al.*, 2002_2).

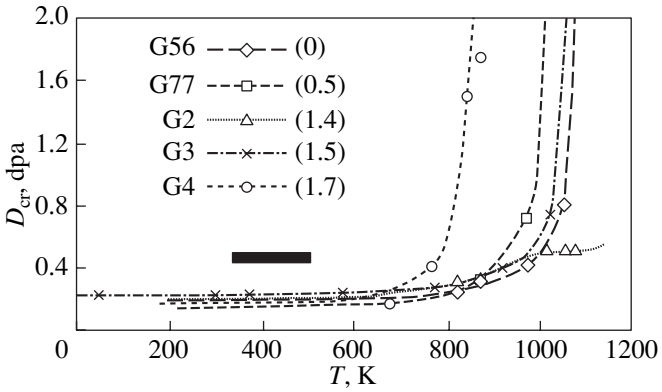

Fig. 17. Temperature dependence of the critical dose for garnet in samples G2, G3, G4, G56, and G77. The black bar indicates the interval of temperatures in HLW underground repositories. Numbers in parentheses are numbers of Zr atoms in the garnet formula.

THE EFFECT OF PHASE STRUCTURE AND COMPOSITION ON RESISTANCE TO RADIATION

The critical temperatures depend on the structure type and irradiation mode (Wang *et al.*, 1999_2; Weber and Ewing, 2002). Upon heavy-ion irradiation, T_{cr} is 20 K for REE zirconates with a pyrochlore structure and increases to 300–700 K for britholite, zirconolite, and zircon (Ewing *et al.*, 1995; Wang *et al.*, 1994, 1999_2). For their structural analogues, T_{cr} depends on the composition of phases. For zirconolites irradiated with 1 MeV Kr^+ ions, the T_{cr} values are 640 K for $CaZrTi_2O_7$, 550 K for $CaZrFeNbO_7$, and 1020 K for $Ca_{0.5}Nd_{0.5}ZrTi_{1.5}Al_{0.5}O_7$ (Wang *et al.*, 2000_1).

The compositional dependence of radiation resistance was also determined for pyrochlore (Wang *et al.*, 2000_2). Lattice resistance to irradiation with 1 MeV Kr ions at 25°C increases from $Gd_2Ti_2O_7$ ($D_{cr} = 2 \times 10^{14}$ Kr$^+$/cm^2) to $Y_2Ti_2O_7$ ($D_{cr} = 4 \times 10^{14}$ Kr$^+$/cm^2), while T_{cr} values are 1100 and 780 K, respectively. Substitution of Zr for Ti also increases the radiation resistance. For example, the critical dose at 25°C is 2.5×10^{14} Kr$^+$/cm^2 for $Gd_2Ti_2O_7$ and $Gd_2Ti_{1.5}Zr_{0.5}O_7$ (Wang *et al.*, 1999_1), while the respective T_{cr} values are 1000 and 850 K. Thus, the second phase in more resistant to radiation (Table 9). The D_{cr} value increases with further substitution of Zr for Ti and is 6×10^{14} ions/cm^2 for pyrochlore Gd_2TiZrO_7, with a corresponding decrease in T_{cr} to 400 K. The Gd zirconate $Gd_2Zr_2O_7$, with a pyrochlore structure, could not be amorphized even at a very large irradiation dose of 7×10^{15} Kr$^+$/cm^2 at low temperature (20–30 K). This could be related to a high rate of restoration of the damaged structure.

An increase in the energy and mass of the ion used for irradiation decreases the critical dose (at a constant

Table 9. Critical doses of ion irradiation (in 10^{14} Kr$^+$/cm^2) for zirconolite (1, 2), perovskite (3, 4), and pyrochlore (5–9) at various temperatures

Formula	20–30 K	300 K	475 K	675 K	923–973 K	Reference
1. $Ca_{0.75}Gd_{0.5}Zr_{0.75}Ti_2O_7$	3.3	6.8	16	>600	–	White *et al.*, 1995
2. $CaZrTi_2O_7$	7.1	10	340	>600	–	″
3. $Ca_{0.8}Gd_{0.2}TiO_3$	9.7	–	–	–	–	″
4. $CaTiO_3$	–	9.2	–	–	–	Smith *et al.*, 1999
5. $Gd_2Ti_2O_7$	2	2.5	2.5	2.5	7	Wang *et al.*, 1999_1
6. $Gd_2Ti_{1.5}Zr_{0.5}O_7$	–	2.5	2.5	4	30	″
7. Gd_2TiZrO_7	–	6	>60	–	–	″
8. $Gd_2Ti_{0.5}Zr_{1.5}O_7$	>40	–	–	–	–	″
9. $Gd_2Zr_2O_7$	>70	>90	–	–	–	″

Table 10. Compositions of pyrochlore and britholite (wt %), average of 5–10 analyses

Components	1 (Pyr)	4 (Pyr)	5 (Pyr)	518 (Pyr)	626 (Pyr)	644 (Pyr)	8 (Br)
Na_2O	7.1	<D.l.	<D.l.	<D.l.	6.3	7.3	<D.l.
CaO	15.6	1.7	3.0	2.1	10.6	13.1	16.7
SrO	<D.l.	<D.l.	<D.l.	<D.l.	<D.l.	<D.l.	<D.l.
Y_2O_3	″	9.5	7.1	″	″	″	″
La_2O_3	″	<D.l.	<D.l.	5.1	<D.l.	<D.l.	10.8
Ce_2O_3	″	″	″	2.3	3.1	3.3	27.1
Pr_2O_3	″	″	″	<D.l.	<D.l.	<D.l.	2.0
Nd_2O_3	″	″	″	5.1	″	″	10.7
Sm_2O_3	″	1.8	1.5	<D.l.	″	″	<D.l.
Gd_2O_3	″	2.2	2.5	″	″	″	″
Dy_2O_3	″	1.6	1.3	″	″	″	″
UO_2	<0.6	7.3[1] (3.6–11.5)[2]	9.0 (5.7–14.1)	3.0 (1.2–4.2)	7.5 (5.7–10.0)	6.8 (6.2–7.1)	<0.6
ThO_2	0.7[1] (<0.6–1)[2]	<0.9	<0.9 (<0.9–1.1)	0.9 (<0.8–1.3)	<0.6	<0.8	4.1 (3.0–5.3)
PbO	<D.l.	4.5	3.9	1.4	0.7	1.4	<D.l.
FeO	″	0.9	3.0	3.2	<D.l.	<D.l.	″
Nb_2O_5	68.0	52.7	51.9	64.0	57.7	55.7	″
Ta_2O_5	<D.l.	7.2	7.7	3.5	2.3	3.6	″
TiO_2	2.7	3.9	2.3	9.5	11.8	8.7	″
SiO_2	<D.l.	6.7	6.8	<D.l.	<D.l.	<D.l.	21.6
P_2O_5	″	<D.l.	<D.l.	″	″	″	3.0
F	5.9	″	″	″	″	″	4.0

Note: D.l., detection limit. [1] Average value. [2] Range.

temperature) and increases T_{cr}. For pyrochlore $(Gd_{0.95}Ca_{0.05})_2Ti_2O_{6.9}$ at 420 K, the D_{cr} value decreases from 8×10^{14} ions/cm^2 (irradiation with Ar^+ ions with energies of 0.6 MeV) to 2×10^{14} (1 MeV Kr^+) and 1×10^{14} ions/cm^2 (1.5 MeV Xe^+). The T_{cr} values correspondingly increase from 950 to 1100 and 1300 K (Wang *et al.*, 1999_2). The difference in the values of D_{cr} and, particularly, T_{cr} on irradiation of britholite $Ca_2La_8(SiO_4)_6O_2$ with Ne^+ (0.8 MeV) and Kr^+ (1.5 MeV) was described in (Ewing *et al.*, 1995). The lattice damage increases with increasing ion mass and energy; thus, lattice restoration requires a higher temperature. In general, T_{cr} values upon ion irradiation are higher by 150–400° than those obtained upon αdecay of actinides in a matrix structure (Weber and Ewing, 2002). The dependence of radiation resistance on the mode of ion irradiation complicates the use of these experimental data for estimating the resistance of matrices with real actinides. The study of natural minerals clarifies some aspects of this problem.

RADIATION DAMAGE IN NATURAL MINERALS

Many actinide matrices have analogues among natural radioactive minerals (Table 4) that have experienced significant radiation impact due to Th and U decay. The study of these minerals helps us to predict HLW matrix behavior in the conditions of an underground repository and refine data on radiation resistance obtained by ion irradiation. Amorphization of lattices of natural radioactive minerals (metamict mineral formation) is described in many publications. Such data have been obtained for pyrochlore (*Mineraly* …, 1967; Krivokoneva and Sidorenko, 1971; Lumpkin *et al.*, 1986, 2001; Giere, 2000; Giere *et al.*, 2001; Yudintseva, 2002), zirconolite (Ewing and Wang, 1992; Lumpkin *et al.*, 1994, 1998_2; Hart *et al.*, 1996), perovskite (Sinclair and Ringwood, 1981; Lumpkin *et al.*, 1998_1), brannerite (Lumpkin *et al.*, 2000), titanite (Vance and Metson, 1985; Hawthorne *et al.*, 1991), zircon-group minerals (Murakami *et al.*, 1991; Lapina and Yudintsev, 1999), and britholite (Gong *et al.*, 1997).

We studied pyrochlores from alkaline rocks of the Vishnevogorskii-Il'menogorskii Massif (Southern Urals, 280–300 Ma) and Khibina Massif (Kola Peninsula, 380–400 Ma), as well as britholite from the Burpala Massif (Eastern Siberia, 320 Ma). The mineral compositions were analyzed on an electron microscope with EDS, their structures were studied using X-ray powder diffraction and transmission electron microscopy, and thermal analysis was performed on a Derivatograf unit. In order to restore the damaged crystal

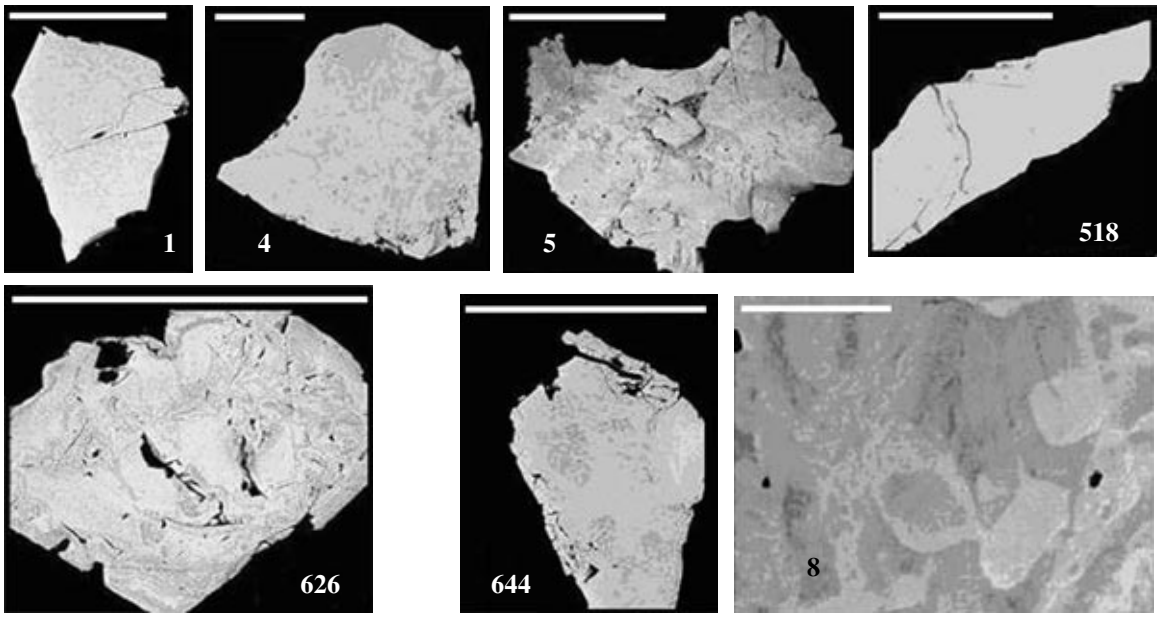

Fig. 18. BSE images of initial samples of pyrochlore and britholite (sample 8). Bars are equal to 20 μm (sample 8), 100 μm (sample 1), 200 μm (samples 4, 518, 626, and 644), and 1000 μm (sample 5).

structures, the samples were annealed for 6 h at 800 and 1200°C (pyrochlores) or 650 and 800°C (britholite). After such treatment, the chemical compositions were analyzed again and new X-ray and electron diffraction patterns were obtained for the annealed samples.

According to SEM data, pyrochlores contain 0.6–10.3 wt % U and 0.6–0.9 wt % Th. Britholites contain <0.6 wt % U and 3.0–5.3 wt % Th (Table 10). Most samples except for samples 1 and 518 are inhomogeneous (Fig. 18), and radioactive element concentrations can differ by several times in different parts of grains. The totals for pyrochlore analyses decrease from 98–100% for crystalline varieties to 85% in amorphized varieties. The total for britholite range from 95 to 98%. Deviation from 100% may be related to incorporation of water in minerals. The formulas were calculated for tetravalent U and bivalent Fe and Mn. The pyrochlore formula is calculated for two cations at the $B^{[6]}$ site, while the britholite formula is calculated for a total negative charge of –50 (Table 11).

The study of pyrochlore revealed three types of X-ray diffraction patterns, corresponding to different stages of destruction (Fig. 19). Type 1 (sample 1) is characterized by complete set of well-pronounced reflexes typical of the pyrochlore structure. X-ray diffraction pattern type 2 (sample 518) shows a lower intensity and larger width of the main peaks (*hkl* = 222, 440, 622), while the less intensive peaks (511, 444) disappear. X-ray diffraction pattern type 3 (samples 626 and 644) does not reveal any reflexes, which indicates complete destruction of the crystal lattice. Similar changes are characteristic of the electron diffraction patterns (Fig. 20). Dotty reflexes (sample 1) become blurred (sample 518) with increasing irradiation dose and degree of damage. The X-ray amorphous samples 626 and 644 show broad rings (halos) around the central reflex of the electron beam in the electron diffraction pattern. The pyrochlore of sample 4 and britholite of sample 8

Table 11. Formulas calculated for two cations in the $B^{[6]}$ site for pyrochlore and for a total negative charge of –50 for britholite

Sample	Formulas
1 (Pyr)	$(Na_{0.85}Ca_{1.02}Th_{0.01})(Nb_{1.87}Ti_{0.13})O_{5.83}F_{1.12}$
4 (Pyr)	$(Ca_{0.10}Fe_{0.04}Pb_{0.06}Y_{0.29}Sm_{0.03}Gd_{0.04}Dy_{0.03}U_{0.09})(Nb_{1.35}Ta_{0.11}Ti_{0.16}Si_{0.38})O_{5.71}$
5 (Pyr)	$(Ca_{0.18}Fe_{0.15}Pb_{0.06}Y_{0.24}Sm_{0.03}Gd_{0.05}Dy_{0.03}U_{0.12})(Nb_{1.37}Ta_{0.13}Ti_{0.10}Si_{0.40})O_{5.86}$
518 (Pyr)	$(Ca_{0.12}Fe_{0.14}Pb_{0.03}La_{0.10}Ce_{0.05}Nd_{0.1}U_{0.04}Th_{0.01})(Nb_{1.55}Ta_{0.06}Ti_{0.39})O_{5.54}$
626 (Pyr)	$(Na_{0.68}Ca_{0.64}Pb_{0.01}Ce_{0.06}U_{0.10})(Nb_{1.46}Ta_{0.04}Ti_{0.50})O_{6.04}$
644 (Pyr)	$(Na_{0.87}Ca_{0.86}Pb_{0.03}Ce_{0.07}U_{0.09})(Nb_{1.54}Ta_{0.06}Ti_{0.40})O_{6.39}$
8 (Br)	$(Ca_{4.61}La_{1.03}Ce_{2.56}Pr_{0.19}Nd_{0.99}Th_{0.24})(Si_{5.57}P_{0.65})O_{23.38}F_{3.24}$

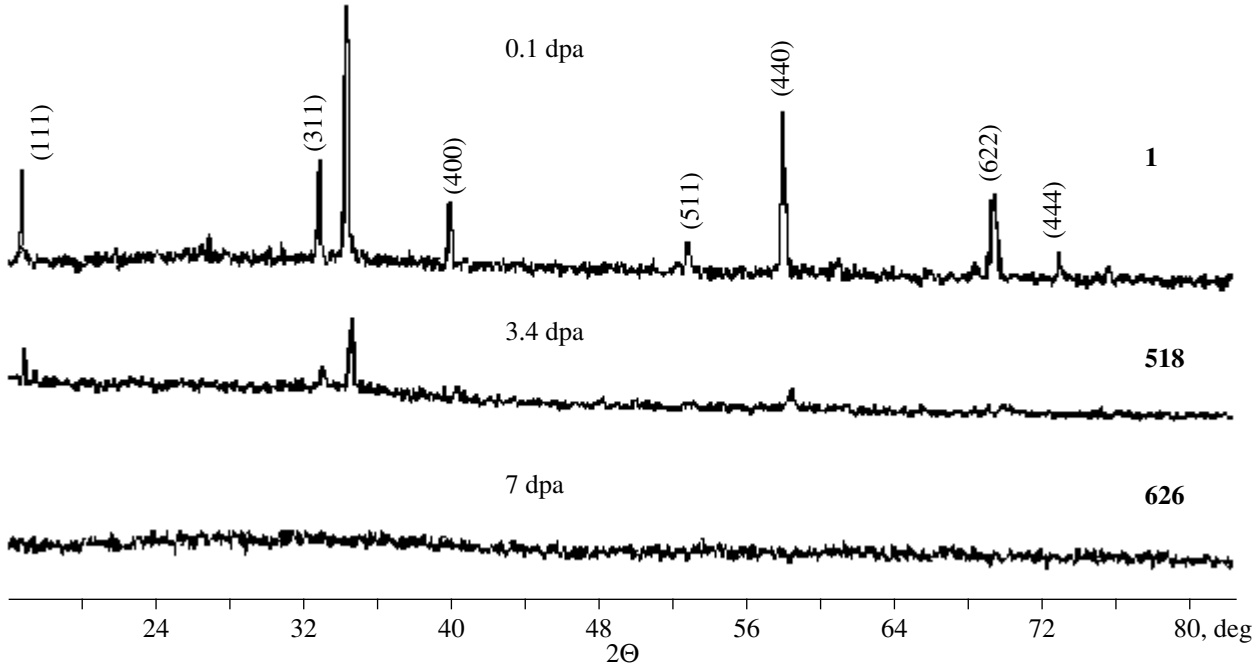

Fig. 19. Changes in X-ray diffraction patterns of pyrochlore (samples 1, 518, and 626) with increasing amorphization grade. Shown are indices of lattice planes and irradiation doses.

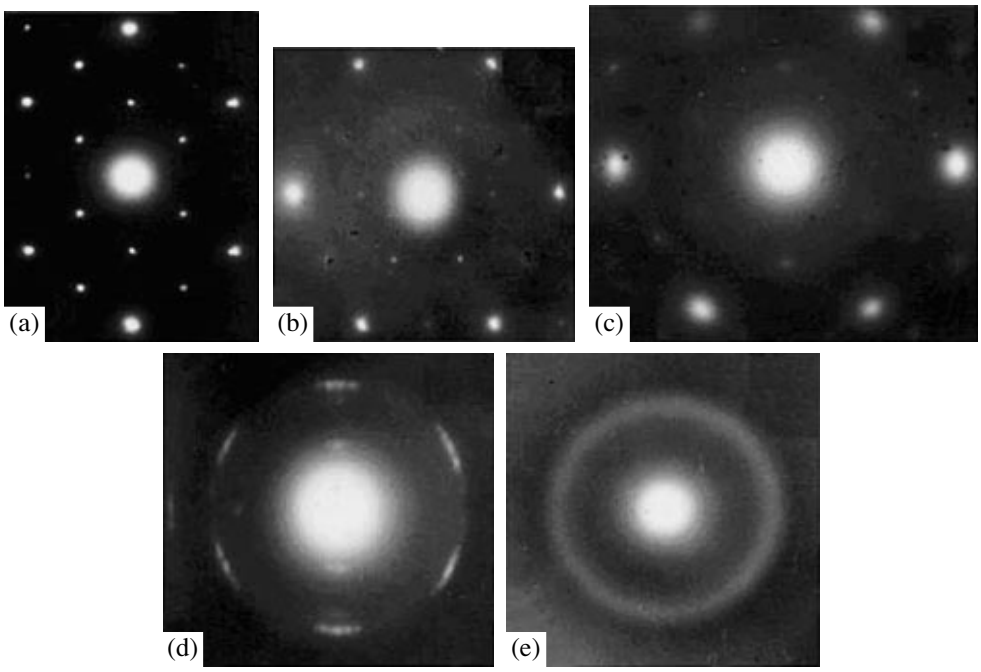

Fig. 20. Stages of destruction of the pyrochlore crystal lattice with increasing irradiation dose, shown in electron diffraction patterns. (a, b) Sample 1; (c) sample 518; (d) sample 4; (e) sample 626.

show dotty and ring-shaped electron diffraction patterns simultaneously. These data indicate that domains with different degrees of damage occur together, which is probably related to inhomogeneous distribution of radioactive elements (Table 10).

The curves of differential thermal analysis show endothermic and exothermic peaks. The former are related to phase dehydration; the latter, with restoration of phase structures. Water escapes at 180°C, while the structures are restored at 380°C (sample 626) and

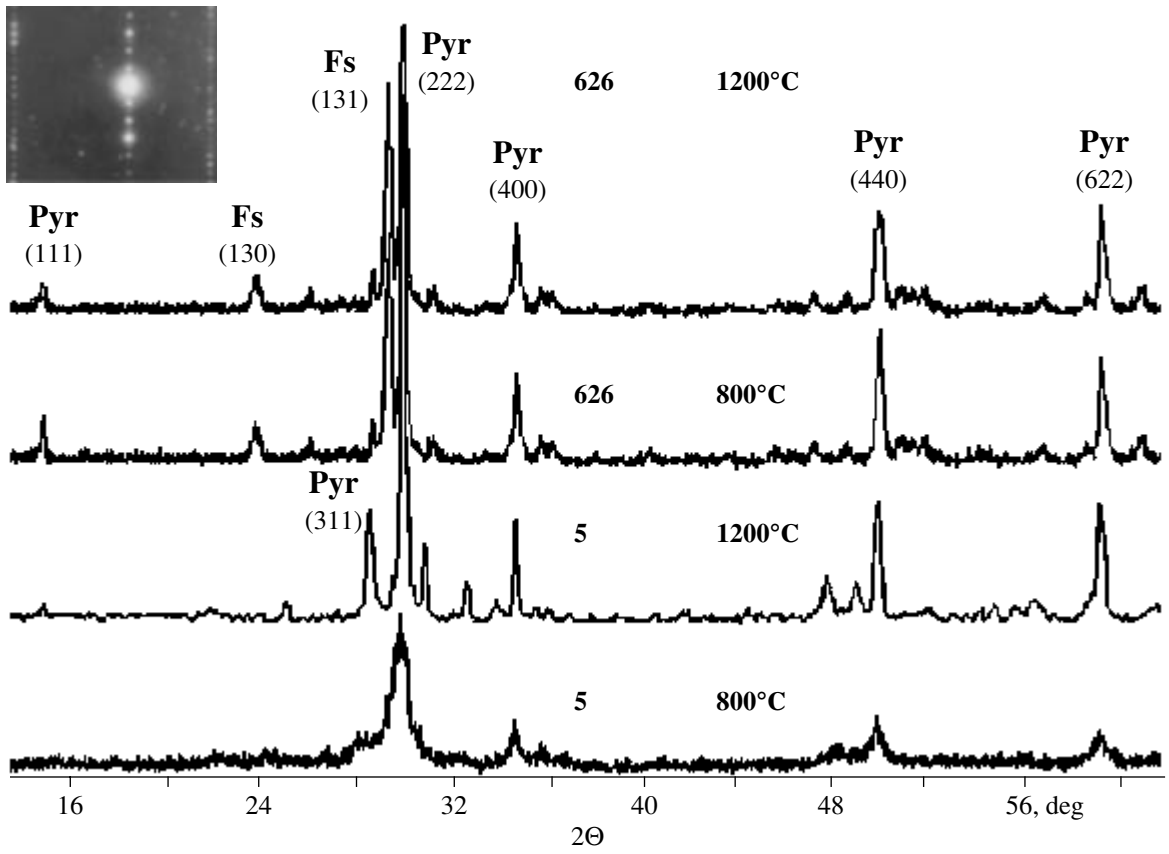

Fig. 21. X-ray diffraction patterns of samples 626 and 5 after annealing for 6 h at 800 and 1200°C. *Pyr* is pyrochlore (indices of lattice planes are shown in parentheses); *Fs* is fersmite. The inset in the upper left part of the figure shows the electron diffraction pattern for fersmite.

700°C (sample 5). The curve for sample 5 reveals an additional exothermic effect at 420°C. Weight losses on annealing are 6.7 and 11.4% for these samples.

Annealing at 800°C for 6 h resulted in partial (sample 5) or complete (sample 626) restoration of pyrochlore structures (Fig. 21). This is consistent with data of thermal analysis demonstrating different temperatures of structural restoration of pyrochlore in these samples. In addition to pyrochlore, sample 626 contains a phase identified by X-ray diffraction and TEM (Figs. 21, 22; Table 12) as fersmite, a mineral of the euxenite group with orthorhombic symmetry (*Pcan*, $Z = 4$) and the theoretical formula $CaNb_2O_6$. The SEM analysis of this mineral resulted in the following real formula: $(Ca_{0.83}Ce_{0.03}La_{0.03})(Nb_{1.79}Ti_{0.18}Ta_{0.03})O_{5.85}$. The annealed sample shows an inhomogeneous distribution of pyrochlore and fersmite within single grains (Fig. 22). Fersmite apparently formed in areas enriched in Nb and Ca; pyrochlore, in areas with elevated U contents. Some other phases (dark patches in SEM images) could form on annealing, because the composition of the initial material cannot be accurately recalculated to the measured compositions of fersmite and pyrochlore (Table 12).

The X-ray diffraction pattern of sample 5 annealed at 800°C shows all main reflexes typical of the pyrochlore structure (Fig. 21). The sample compositions before and after annealing are equal within the analytical error. However, judging by the imperfect shapes of reflexes in the X-ray diffraction pattern, the structure is not completely restored under these conditions. Heating to 1200°C accomplishes the structural restoration in sample 5. Moreover, a new phase appears in a small amount, which is indicated by weak reflexes not related to pyrochlore.

The formation of two new phases instead of one initial phase is a normal process occurring on annealing of metamict samples (Ewing and Ehlmann, 1975). It could be related to different conditions of formation of the initial mineral and its treatment in the laboratory. The latter is performed at a higher temperature and oxidation potential, under atmospheric pressure, and without volatile components. The formation of these phases could be also caused by chemical transformation of the primary mineral due to radioactive decay and various metasomatic processes. If the primary mineral has not been completely destructed, only one phase, with a lattice similar to the primary mineral lattice, normally forms on annealing. If an amorphous sample is

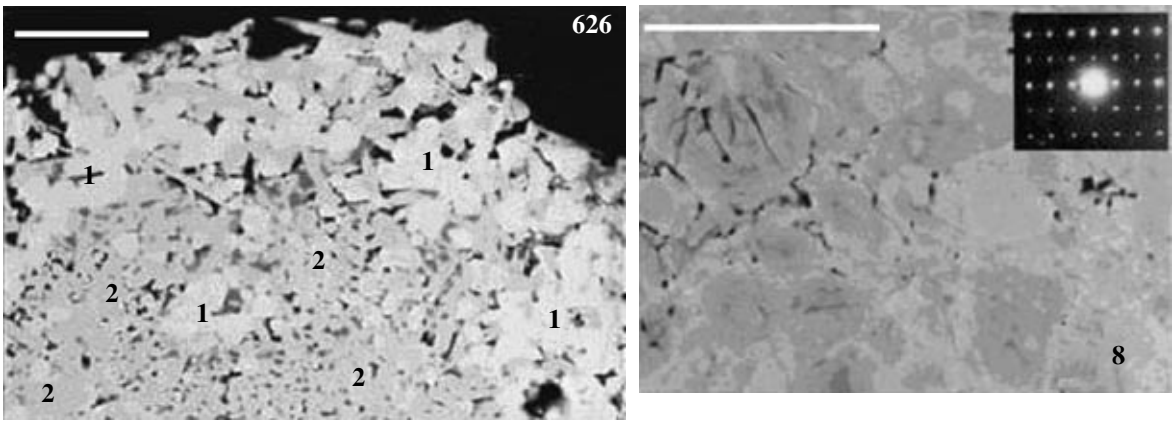

Fig. 22. BSE images of pyrochlore (sample 626) and britholite (sample 8) after annealing for 6 h at 1200°C (pyrochlore) and 650°C (britholite). (1) Pyrochlore; (2) fersmite. The bars are equal to 20 μm (sample 626) and 40 μm (sample 8). The inset in the right image shows the electron diffraction pattern for britholite.

annealed, several phases with different structures frequently form.

The X-ray diffraction pattern of the initial britholite has two broad peaks, asymmetric between 16° and 36° and symmetric between 42° and 52° (Fig. 23). Weak reflexes within these intervals indicate that the primary crystal structure is partially preserved. The thermal analysis curve shows an exothermic peak at 500°C

Table 12. Compositions of samples before and after annealing (average of 5–10 samples, Σ = 100 wt %)

Elements, wt %	Sample 626 (pyrochlore)			Sample 5 (pyrochlore)		Sample 8 (britholite)	
	initial	annealed		initial	annealed	initial	annealed
	pyrochlore*	pyrochlore	fersmite	pyrochlore	pyrochlore	britholite	britholite
Na_2O	6.7	2.8	<D.l.	<D.l.	<D.l.	<D.l.	<D.l.
CaO	12.0	9.5	14.9	3.0	3.3	16.7	16.8
FeO	<D.l.	0.6	<D.l.	3.0	3.5	<D.l.	<D.l.
Y_2O_3	″	″	″	7.1	7.0	″	″
La_2O_3	″	″	1.5	<D.l.	<D.l.	10.8	10.4
Ce_2O_3	3.1	3.1	1.6	″	″	27.1	27.2
Pr_2O_3	<D.l.	<D.l.	<D.l.	″	″	2.0	1.9
Nd_2O_3	″	″	″	″	″	10.7	10.6
Sm_2O_3	″	″	″	1.5	1.8	<D.l.	<D.l.
Gd_2O_3	″	″	″	2.5	3.2	″	″
Dy_2O_3	″	″	″	1.3	1.8	″	″
ThO_2	″	″	″	<D.l.	<D.l.	4.1	4.4
UO_2	7.5	14.4	″	9.0	10.1	<D.l.	<D.l.
PbO	0.7	<D.l.	″	3.9	3.6	″	″
TiO_2	11.8	14.0	4.6	2.3	3.8	″	″
SiO_2	<D.l.	<D.l.	<D.l.	6.8	6.9	21.6	21.8
P_2O_5	″	″	″	<D.l.	<D.l.	3.0	3.1
Ta_2O_5	3.3	2.7	1.3	7.7	5.8	<D.l.	<D.l.
Nb_2O_5	57.7	53.0	76.1	51.9	49.3	″	″
F	<D.l.	<D.l.	<D.l.	<D.l.	<D.l.	4.0	3.8

Note: D.l., detection limit.
* Scanning over a grain.

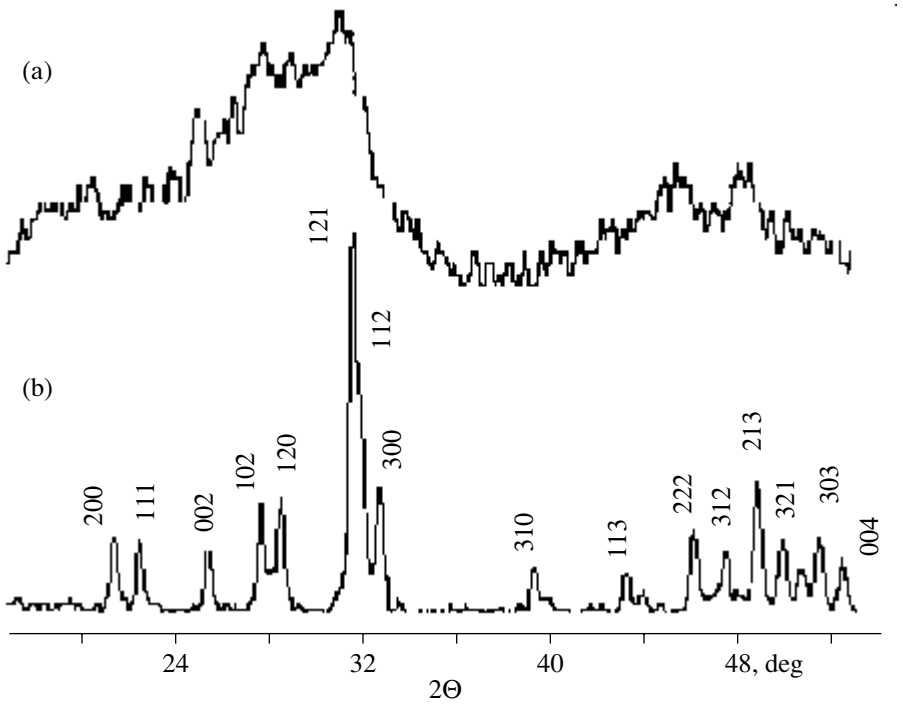

Fig. 23. X-ray diffraction patterns of britholite (Cu irradiation) in sample 8: (a) initial; (b) after annealing for 6 h at 650°C. Numbers are indices of lattice planes.

related to structural restoration. Weight loss on annealing is 2 wt %, indicative of weak hydration of the initial sample. Heating resulted in complete structural restoration, with the appearance of all reflexes typical of britholite. X-ray diffraction patterns of sample 8 heated to 650 and 800°C have similar shapes, which indicates that the structure was already restored at 650°C. Chemical heterogeneity (Fig. 22) typical of the initial mineral is retained after its annealing. No other phases have been detected.

Destruction of natural minerals is related to decay of radioactive elements. The irradiation dose can be characterized by the number of α decay events per gram of material and depends on the content of radioactive elements in the mineral and its age. One ^{238}U atom decays to produce one ^{206}Pb atom and eight α particles, while one ^{232}Th decay event generates one ^{208}Pb atom and six α particles. The irradiation dose can be calculated by the equation

$$D = 8N_{238}(e^{\lambda_{238}t} - 1) + 6N_{232}(e^{\lambda_{232}t} - 1),$$

where N_{238} and N_{232} are the numbers of U and Th atoms in one gram of a mineral, t is the mineral age in years, and λ_{238} and λ_{232} are the ^{238}U and ^{232}Th decay constants (Lumpkin *et al.*, 1986).

We calculated accumulated irradiation doses for all samples studied (Table 13). Amorphization of natural

Table 13. Irradiation doses accumulated in pyrochlores and britholite (sample 8)

Sample	Content, wt %		T, 10^8 yr	Dose, 10^{19} α decay events/g	Dose, dpa
	^{238}U	^{232}Th			
1	<0.6	0.7[1] (<0.6–1.0)[2]	3	0.14[1] (<0.1–0.18)[2]	0.1[1] (<0.05–0.15)[2]
518	3.0[1] (1.2–4.2)[2]	0.9 (<0.8–1.3)	4	3.5 (1.4–4.8)	3.4 (1.3–4.6)
644	6.8 (6.2–7.1)	<0.6	4	7.8 (7–8)	6.6 (6–7)
4	7.3 (3.6–11.5)	<0.6	2.8	6.0 (2.8–9)	6.5 (3–10)
626	7.5 (5.7–10)	<0.6	4	8.5 (6.7–11)	7.0 (5.8–9.5)
5	9.0 (5.7–14.1)	<0.6	2.8	7.5 (5–11)	8.0 (5.4–12)
8	<0.6	4.0 (3.0–5.3)	3.2	1.1 (0.8–1.2)	0.9 (0.6–1.1)

[1] Average value. [2] Range.

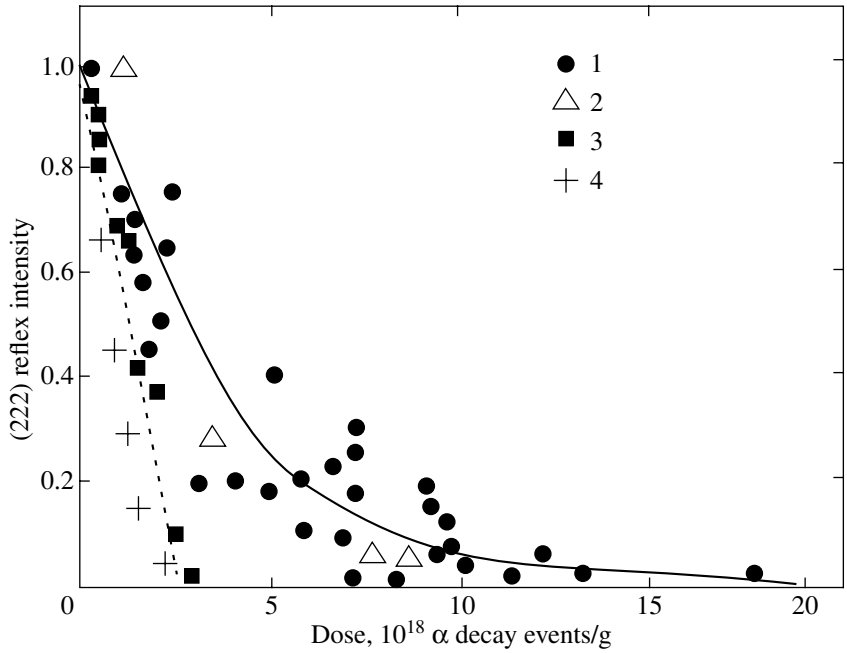

Fig. 24. Change in intensity of the *hkl* = 222 reflex in the X-ray diffraction patterns of natural (U,Th)-bearing pyrochlores (1, 2) and their synthetic (Pu,Cm)-bearing analogues (3, 4) as function of theaccumulated irradiation dose. (1) Lumpkin and Ewing (1988); (2) data of the authors; (3) Weber *et al.*, 1986; (4) Burakov and Anderson, 2001.

pyrochlores occurs at irradiation doses from 7×10^{18} to 2×10^{19} α decay events/g (Fig. 24). The critical dose is several times smaller [$(2–3) \times 10^{18}$ α decay events/g] for synthetic titanates with a pyrochlore structure and incorporated short-lived isotopes ^{238}Pu and ^{244}Cm. Such a difference is related to reparation of structural defects in natural minerals over their long lifetime (several hundred million years). This process is stimulated by elevated temperature, which could be related to metamorphism. The radiation resistance of the britholite structure (sample 8) is 10^{19} α decay events/g (Table 13) and is close to published data (Gong *et al.*, 1997).

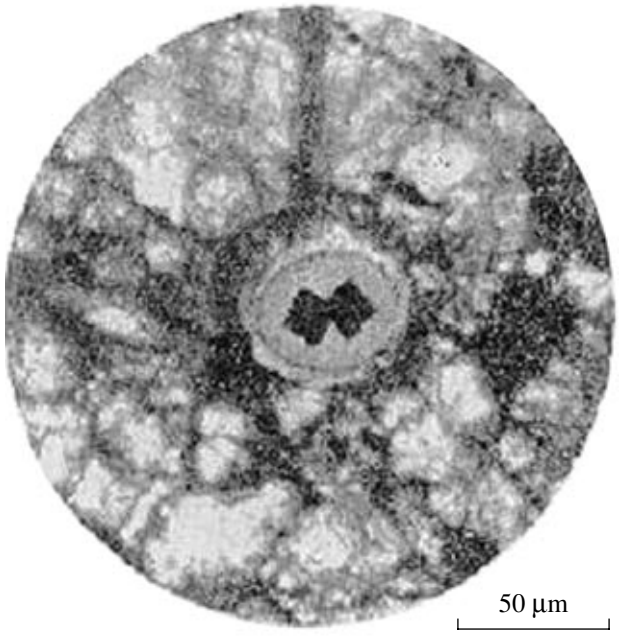

Fig. 25. A zone of chlorite-like aggregate around a uraninite inclusion in natural andradite (Karpenko, 1966). Transmitted light. Parallel nicols.

Natural garnets are free of radioactive elements (Jaffe, 1951). Thus, the study of natural garnets, unlike potential actinide-bearing phases (zirconolite, pyrochlore, britholite), cannot help in estimation of the radiation resistance of synthetic phases with a garnet structure. The single relevant paper known to us is devoted to study of andradite alteration under a radiation impact produced by uraninite inclusions (Karpenko, 1966). Uraninite grains are surrounded by a zone of a chlorite-like mineral about 20 μm wide, which corresponds to α particle tracks (Fig. 25). Such zones, termed pleochroic halos, normally surround inclusions of radioactive accessory minerals (monazite, thorite, uraninite) in biotite and tourmaline.

COMPARISON OF DATA ON THE RADIATION RESISTANCE OF ACTINIDE-BEARING MATRICES IRRADIATED BY DIFFERENT METHODS

Data on radiation resistance have been obtained for many potential actinide-bearing matrices using different methods of internal or external irradiation (Ewing and Wang, 1992; Ewing *et al.*, 1995; Ewing, 1999; Weber and Ewing, 2002). In order to compare these

Table 14. Radiation-induced changes in phase properties (*Radioactive...*, 1988; Ewing *et al*., 1995; Weber *et al*., 1998; Ewing, 1999; Weber and Ewing, 2002; data of the authors)

Synthetic phase (natural analogue)	D_{cr}, dpa (at 25°C)	T_{cr}, K	Expansion, rel. %	Excess energy, J/g
$REEPO_4$ (monazite)	>1	<300[(1)]	No data	>30
$ZrSiO_4$ (zircon)	0.4–0.6	600[(1)]/900[(2)]	16–18	320
$CaTiSiO_5$ (titanite)	0.3–0.4	No data	No data	No data
$Ca_2REE_8(SiO_4)_6O_2$ (britholite)	0.3–0.6	300[(1)]/950[(2)]	5	130
$CaTiO_3$ (perovskite)	>0.7	250[(1)]/420[(2)]	>8	No data
$CaZrTi_2O_7$ (zirconolite)	0.3–0.5	>300[(1)]/640[(2)]	5–6	50–130
$Gd_2Ti_2O_7$ (no)	0.2–0.4	600[(1)]/1000[(2)]	5	50–130
$CaPuTi_2O_7$ (no)	0.2	600[(1)]	5–6	50–60
$CaUTi_2O_7$ (betafite)	0.2	600[(1)]	5–6	50–60
$Gd_2Zr_2O_7$ (no)	>10	<20[(2)]	No data	No data
$[(Ca,Mn,Gd,Zr,U)_3(Ti,Mn)_6(Ti,Fe,Al)_2O_{22-x}]$ (murataite)	0.2	(800–1000)[(2)] (depends on composition)	″	″
$[(Ca,Gd,U)_3(Zr,Fe)_2(Si,Fe,Al)_3O_{12}]$ (garnet (kimzeyite))	0.2	(900–1100)[(2)] (depends on composition)	″	″
UTi_2O_6 (brannerite)	0.1	No data	″	″

[(1)] During α decay.
[(2)] As a result of ion irradiation.

data, we should express the values of D_{cr} in common units of radiation impact on crystal structure. The number of displacements per atom of a structure (dpa) is normally used as such a unit. A dose of 1 dpa means that every atom was displaced from its initial site. Equivalent values expressed in these units can be calculated for various types of radiation, on the basis of specific features of its interaction with a crystal lattice. To convert doses of α decay into the number of displacements per atom (dpa), one should use the following formula: $1500 \times (D \times M) : (N_f \times N_A)$, where 1500 is the average number of collisions with lattice atoms after one decay event, D is the α decay dose, M is the molecular weight of the compound, N_f is the number of atoms in the formula, and N_A is Avogadro's number (Lumpkin *et al.*, 1994; Gong *et al.*, 1997). Doses of heavy ion irradiation are converted with special computer codes (Ziegler *et al.*, 1985).

For most phases, including pyrochlore, garnet, murataite, and zirconolite, a dose of ion irradiation of 10^{14} Kr^+/cm^2 provides 0.08–0.12 dpa (0.1 dpa, on average). Amorphization of the phases studied occurs at 0.3 dpa for zirconolite; 0.2 dpa for pyrochlore, garnet, and murataite; and only 0.1 dpa for brannerite (at 25°C). Using the above formula, we converted the values of radiation resistance from the number of displacements per atom (dpa) into the number of α decay events per gram. Thus, the critical dose for murataite was estimated at 3×10^{18} α decay events/g, and the amorphization time, at 600–700 years at a hypothetical ^{239}Pu content of 10 wt %. It can be supposed that the central, actinide-richer parts of murataite grains will be amorphized in shorter periods than the margins, which are poorer in these elements. The calculated times of complete amorphization vary from 500 years for brannerite to 2000 years for zirconolite and pyrochlore. If the wastes contain short-lived actinides (^{238}Pu, ^{241}Pu, and ^{241}Am), the matrix structure will be amorphized in an even shorter period. For example, complete amorphization of the titanate pyrochlore with 8.7 wt % ^{238}Pu (Burakov *et al.*, 2001; Lukinykh *et al.*, 2001) occurred in <2 years. Its radiation resistance is about 0.2 dpa.

The calculated values are close to previous estimates (0.3–0.5 dpa for zirconolite $CaZrTi_2O_7$ and 0.2–0.4 dpa for titanate pyrochlores) (Table 14). Values of 0.3–0.4 dpa were determined for synthetic zircon and britholite $Ca_2La_8(SiO_4)_6O_2$ and Sr perovskite $SrTiO_3$ (Weber and Ewing, 2002). The structures of phosphate matrices are more resistant to radiation. The critical dose of the $NaPu_2PO_4$ phase with a kosnarite structure is about 1 dpa at 25°C (Orlova *et al.*, 2002). The radiation resistance of monazite $LuPO_4$ with 1 wt % ^{244}Cm is still higher (Liu *et al.*, 1998). Its structure was not amorphized after 17 years at a cumulative dose of 1.2×10^{19} α decay events/g, corresponding to 1.3 dpa.

Cubic oxides $REE_2Zr_2O_7$ (REE = La, Nd, Sm, Gd) and ZrO_2 are the most resistant to radiation among the known actinide-bearing matrices. Gd and Nd zirconates with a pyrochlore structure were not amorphized at irradiation doses of 4×10^{15} Xe^+/cm^2 or 7×10^{15} Kr^+/cm^2 and very low temperatures (20–30 K) (Wang *et al.*, 1999_1; Lian *et al.*, 2002_1). The critical dose for $Gd_2Zr_2O_7$ is >15 dpa or 3×10^{20} α decay events/g. A matrix with 10 wt % ^{239}Pu will accumulate such a dose over many

millions of years (Table 2). High radiation resistance was also found for cubic ZiO_2 with 9.9 wt % ^{238}Pu (Burakov and Anderson, 2001). The high resistance of these materials to radiation is related to a high reparation rate of radiation damage.

CONCLUSIONS

It was found that critical doses of ion irradiation for actinide-bearing phases at 25°C are as follows (in 10^{14} ions Kr^+/cm^2): 2.9 for zirconolite, 1.8–2.4 for pyrochlore, 1.5–2 for garnet, 1.7–1.9 for murataite, 1.4 for brannerite, and 0.4 for britholite. Murataite varieties with three-, five-, and eightfold fluorite unit cells have similar resistance to radiation. Calculated D_{cr} values for all phases studied range from 0.1 to 0.4 dpa. The amorphization time for their structures at a hypothetical ^{239}Pu concentration of 10 wt % is estimated at 500–2000 yr.

The D_{cr} values at room temperature estimated on ion irradiation or actinide decay are generally similar for most phases (0.2–0.5 dpa) (Ewing, 1995; Ewing *et al.*, 1998; Weber and Ewing, 2002). For example, the structure of the titanate pyrochlore with 8.7 wt % ^{238}Pu was amorphized in two years at an irradiation dose of $(2.5–2.7) \times 10^{18}$ α decay events/g, corresponding to about 0.2 dpa (Lukinykh *et al.*, 2001; Burakov *et al.*, 2001). The critical dose for the $Gd_2Ti_2O_7$ phase with 10 wt % ^{239}Pu is estimated at 3×10^{18} α decay events/g (0.2 dpa), which will be accumulated over about 1000 yr (Weber and Ewing, 2002). Amorphization increases the rate of actinide leaching by 10–50 times.

The critical temperature at which a crystal structure is stable at any doses depends on the irradiation mode. For phases irradiated by ions, the critical temperatures are higher by 100–400° than those for the same phases irradiated during actinide decay in the matrix structure (Weber and Ewing, 2002). Because of heating due to radioactive decay, the matrix temperature will be maintained at 300–400°C for a few tens or hundreds of years (Weber *et al.*, 1997; Sizgek, 2001). Such temperatures can be reached at high contents of short-lived fission products. The temperature will be lower if the contents of fission products are low or they are absent (e.g., in actinide fractions of HLW and plutonium). It will be close to temperatures determined by the geothermal gradient and, depending on the location and depth of the HLW repository, will reach 50–200°C. According to (Lumpkin *et al.*, 1996; Weber and Ewing, 2002), the temperature can vary from 50 to 300°C. Temperatures from 100 to 450°C are assumed for conditions in deep-well repositories (Lumpkin *et al.*, 1998_2; Giere, 2000). Critical temperatures of amorphization due to actinide decay are within these intervals for most phases. Therefore, the thermal conditions of an underground repository can significantly affect the radiation resistance of structures of HLW confinement matrices.

Natural zirconolite and pyrochlore structures are preserved at irradiation doses of 2×10^{19} to 10^{20} α decay events/g (Sinclair and Ringwood, 1985; Lumpkin *et al.*, 1986). Critical doses of complete amorphization range from 1 to 6 dpa (Ewing and Wang, 1992; Lumpkin *et al.*, 1986; data of the authors) and occasionally reach 20 dpa (Lumpkin *et al.*, 1986). This is significantly higher than the values obtained by irradiation of phases by heavy ions or during decay of short-lived actinide admixtures in the lattice (Fig. 24). In addition to structural damage, the natural minerals undergo chemical transformations, e.g., accumulation of actinide fission products (lead), changes in element oxidation state, and hydration. Nevertheless, these minerals can securely confine actinides under attack of aqueous solutions (Ringwood, 1985; Giere *et al.*, 2001; Lumpkin *et al.*, 2001).

The amorphous state is metastable, and the displaced atoms gradually return to their initial sites. The rate of this process depends on the crystallochemical features of phases (the energies of interatomic bonds; the nature of atom surroundings) and temperature. Temperature only weakly affects the critical doses for titanates with a pyrochlore structure up to 300°C. In contrast, the critical doses for ZrO_2, REE zirconate, monazite, and britholite rapidly increase even at low temperatures (25–50°C and lower). The deviation of the critical doses and amorphization times of synthetic matrices from those of their natural analogues is generally caused by the complex thermal history of radioactive minerals. Because of rapid restoration of radiation-damaged structures at high temperatures, crystal lattices can be destructed only over several hundred thousand years or more. Thus, long-lived actinide matrices should be stored in deep-well repositories to increase their capability for immobilizing actinides.

ACKNOWLEDGMENTS

We thank L.A. Kochetkova, O.R. Rafal'skaya, B.S. Nikonov, M.I. Lapina, A.V. Mokhov, and A.V. Sivtsov for studying samples by XRD, DTA, SEM, and TEM, as well as M.I. Fedorova, Yu.I. Matyunin, A.G. Ptashkin, O.I. Kir'yanova, and N.P. Mikhailenko for synthesis of matrices. We are grateful to Z.V. Shlyukova and V.S. Kudrin for providing minerals for study.

This study was supported by the Russian Foundation for Basic Research, project no. 02-05-64008, and the US Department of Energy, project no. RC0-20002-SC14.

REFERENCES

Aleksandrova, I.T., Ginzburg, A.I., Kupriyanova, I.I., and Sidorenko, G.A., *Geologiya mestorozhdenii redkikh elementov. Redkozemel'nye silikaty* (Geology of Rare-Element Deposits. Rare Earth Elements), Moscow: "Nedra," 1966.

Bayliss, P., Mazzi, F., Munno, R., and White, T.J., Mineral Nomenclature: Zirconolite, *Mineral. Mag.*, 1989, vol. 53, Part 5, pp. 565–569.

Belov, N.V., Sketches in Structural Mineralogy, *Mineral. Sb. L'vov. Geol. O–va*, 1950, no. 4, pp. 21–34.

Burakov, B.E. and Anderson, E.B., Summary of Pu Ceramics Developed for Pu Immobilization, in *Excess Weapons Plutonium Immobilization in Russia: A Review of LLNL Contract Work*, Livermore: LLNL, 2000, pp. 167–179.

Burakov, B., Anderson, E., Yagovkina, M., *et al.*, Behavior of ^{239}Pu-doped Ceramics Based on Cubic Zirconia and Pyrochlore under Radiation Damage, *Proc. Int. Conf. ACTINIDES-2001*, Hayama, 2001.

Ebbinghaus, B.B., Van Konynenburg, R.A., Ryerson, F.J., *et al.*, Ceramic Formulation for the Immobilization of Plutonium, *Proc. Int. Conf. "Waste Management'98," Tucson*, 1998, CD-version, Paper 65-04.

Ercit, T.S. and Hawthorne, F.C., Murataite, a UB_{12} Derivative Structure with Condensed Keggin Molecules, *Can. Mineral.*, 1995, vol. 33, pp. 1223–1229.

Ewing, R.C., Nuclear Waste Forms for Actinides, *Proc. Natl. Ac. Sci. USA*, 1999, vol. 96, pp. 3432–3439.

Ewing, R.C. and Ehlmann, A.J., Annealing Study of Metamict, Orthorhombic, Rare Earth, AB_2O_6-Type, Nb–Ta–Ti Oxides, *Can. Mineral.*, 1975, vol. 13, Part 1, pp. 1–7.

Ewing, R.C. and Wang, L.M., Amorphization of Zirconolite: Alpha-Decay Event Damage Versus Krypton Ion Irradiation, *Nucl. Instr. Meth. Phys. Research*, 1992, vol. 65, pp. 319–323.

Ewing, R.C., Weber, W.J., and Clinard, F.W., Radiation Effects in Nuclear Waste Forms for High-Level Radioactive Waste, *Progr. Nucl. Energy*, 1995, vol. 29, no. 2, pp. 63–127.

Ewing, R.C., Weber, W.J., and Lutze, W., Crystalline Ceramics: Waste Forms for the Disposal of Weapons Plutonium, *Disposal of Weapon Plutonium. Netherlands*, Kluwer Academic, 1996, pp. 65–83.

Fielding, P.E. and White, T.J., Crystal Chemical Incorporation of High Level Waste Species in Aluminotitanate-Based Ceramics: Valence, Location, Radiation Damage, and Hydrothermal Durability, *J. Mater. Res.,* 1987, vol. 2, no. 3, pp. 387–413.

Geller, S., Crystal Chemistry of the Garnets, *Z. Kristallogr.*, 1967, vol. 125, pp. 1–47.

Giere, R., Minerals as Natural Analogues for Crystalline Nuclear Waste Forms, *A Geochemical and Mineralogical Approach to Environmental Protection. Proc. Int. School Earth and Planet. Sci.*, Siena, 2000, pp. 83–101.

Giere, R., Buck, E.C., Guggenheim, R., *et al.*, Alteration of Uranium-Rich Microlite, *Proc. Symp. "Sci. Bas. Nucl. Waste Management XXIV,"* Warrendale: MRS, 2001, vol. 663, pp. 935–944.

Giere, R., Williams, C.T., and Lumpkin, G.R., Chemical Characteristics of Natural Zirconolite, *Schweiz. Mineral. Petrogr. Mitt.*, 1998, vol. 78, pp. 433–459.

Gong, W.L., Lutze, W., and Ewing, R.C., Zirconia—A Ceramic for Excess Weapons Plutonium Wastes, *Proc. Symp. "Sci. Bas. Nucl. Waste Management XXII,"* Warrendale: MRS, 1999, vol. 556, pp. 63–70.

Gong, W.L., Wang, L.M., Ewing, R.C., *et al.*, Transmission Electron Microscopy Study of α-Decay Damage in Aeshinite and Britholite, *Proc. Symp. "Sci. Bas. Nucl. Waste Management XX,"* Pittsburgh: MRS, 1997, vol. 465, pp. 649–656.

Hart, K.P., Lumpkin, G.R., Giere, R., *et al.*, Naturally-Occurring Zirconolites—Analogues for the Long-Term Encapsulation of Actinides in Synroc, *Radiochim. Acta*, 1996, no. 74, pp. 309–312.

Hawthorne, F.C., Groat, L.A., Raudsepp, M., *et al.*, Alpha-Decay Damage in Titanite, *Am. Mineral.*, 1991, vol. 76, nos. 3–4, pp. 370–396.

Hench, L.L., Clarke, D.E., and Campbell, J., High-Level Waste Immobilization Forms, *Nucl. Chem. Waste Management*, 1984, vol. 5, pp. 149–173.

Ito, J., Silicate Apatites and Oxyapatites, *Am. Mineral.*, 1968, vol. 53, pp. 890–907.

Jaffe, H., The Role of Yttrium and Other Minor Elements in the Garnet Group, *Am. Mineral.,* 1951, vol. 36, nos. 1–2, pp. 133–155.

Karpenko, V.S., Radioactive Halos around Inclusions in Andradite, in *Voprosy prikladnoi radiogeologii* (Problems of Applied Radiogeology), Moscow: Gosatomizdat, 1963, pp. 157–173.

Krivokoneva, G.K. and Sidorenko, G.A., Mechanism of Metamict Transformation of Pyrochlore, *Geokhimiya*, 1997, no. 2, pp. 193–197.

Lapina, M.I. and Yudintsev, S.V., Study of Natural Zircon-Xenotime Assemblages for Estimation of the Actinide Waste Form Stability, *Proc. Symp. "Sci. Bas. Nucl. Waste Management XXII." Warrendale*, MRS, 1999, vol. 556, pp. 785–792.

Laverov, N.P., Gorshkov, A.I., Yudintsev, S.V., *et al.*, New Structural Varieties of Synthetic Murataite, *Dokl. Akad. Nauk*, 1998_1, vol. 363, no. 4, pp. 540–543.

Laverov, N.P., Omel'yanenko, B.I., Yudintsev, S.V., and Nikonov, B.S., Zirconolite as a Matrix for Immobilization of High-Level Radioactive Wastes, *Geol. Rudn. Mestorozhd.*, 1996, vol. 38, no. 5, pp. 387–395.

Laverov, N.P., Sobolev, I.A., Stefanovsky, S.V., *et al.*, Synthetic Murataite: A New mineral for Actinide Immobilization, *Dokl. Akad. Nauk*, 1998_2, vol. 362, no. 5, pp. 670–672.

Laverov, N.P., Yudintsev, S.V., Omel'yanenko, B.I., *et al.*, Murataite Ceramics for the Immobilization of Actinides, *Geol. Rudn. Mestorozhd.*, 1999, vol. 41, no. 2, pp. 99–108.

Laverov, N.P., Yudintsev, S.V., Stefanovsky, S.V., and Jang, Y.N., New Actinide Matrices with a Pyrochlore Structure, *Dokl. Akad. Nauk*, 2001, vol. 381, no. 3, pp. 399–402.

Lian, J., Wang, L.M., Chen, J., *et al.*, Heavy Ion Irradiation of Zirconate Pyrochlores, *Proc. Symp. "Sci. Bas. Nucl. Waste Management XXV," Warrendale*, MRS, 2002_1, vol. 713, pp. 507–512.

Lian, J., Yudintsev, S.V., Stefanovsky, S.V., *et al.*, Ion-Induced Amorphization of Murataite, *Proc. Symp. "Sci. Bas. Nucl. Waste Management XXV," Warrendale*, MRS, 2002_2, vol. 713, pp. 455–460.

Liu, G.K., Luo, J.S., Li, S.T., *et al.*, Self-Radiation Induced Anisotropic Structure Damage in ^{244}Cm-Doped Orthophosphate $LuPO_4$, *Proc. Symp. "Sci. Bas. Nucl. Waste Management XXI." Warrendale*, MRS, 1998, vol. 506, pp. 921–922.

Lukinykh, A.N., Tomilin, S.V., Lizin, A.A., and Bychkov, A.V., Study of Radiation and Chemical Resistance of a Titanate Ceramics for Actinide Immobilization, *Tr. 3 ezhegodnoi vstrechi po koordinatsii i obzoru rossiiskikh rabot v ramkakh dogovorov s Livermorskoi natsional'noi laboratoriei im. Lourensa* (Proc. 3rd Annual Meeting for Coordination and Review of LLNL Contract Work), St. Petersburg, 2002, pp. 270–280.

Lumpkin, G.R., Chakoumakos, B.C., and Ewing, R.C., Mineralogy and Radiation Effects of Microlite from the Harding Pegmatite, Taos County, New Mexico, *Am. Mineral.*, 1986, vol. 71, pp. 569–588.

Lumpkin, G.R., Colella, M., Smith, K.L., *et al.*, Chemical Composition, Geochemical Alteration, and Radiation Damage Effects in Natural Perovskite, *Proc. Symp. "Sci. Bas. Nucl. Waste Management XXI." Warrendale*, MRS, 1998_1, vol. 506, pp. 207–214.

Lumpkin, G.R., Ewing, R.C., Williams, C.T., and Mariano, A.N., An Overview of the Crystal Chemistry, Durability, and Radiation Damage Effects of Natural Pyrochlore, *Proc. Symp. "Sci. Bas. Nucl. Waste Management XXIV." Warrendale*, MRS, 2001, vol. 663, pp. 921–924.

Lumpkin, G.R., Leung, S.H.F., and Colella, M., Composition, Geochemical Alteration, and Alpha-Decay Damage Effects of Natural Brannerite, *Proc. Symp. "Sci. Bas. Nucl. Waste Management XXIII." Warrendale*, MRS, 2000, vol. 608, pp. 461–466.

Lumpkin, G.R., Smith, K.L., Blackford, M.G., *et al.*, The Crystalline–Amorphous Transformation in Natural Zirconolite: Evidence for Long-Term Annealing, *Proc. Symp. "Sci. Bas. Nucl. Waste Management XXI." Warrendale*, MRS, 1996, vol. 506, pp. 215–222.

Lumpkin, G.R., Smith, K.L., Blackford, M.G., *et al.*, Prediction of the Long-Term Performance of Crystalline Nuclear Waste Form Phases from Studies of Mineral Analogues, *Proc. 9th Pacific Basin Nucl. Conf., Sydney*, Austral. Nucl. Assoc., 1994, Nat. Conf. Publ., no. 94/6.

Lumpkin, G.R., Smith, K.L., and Blake, R.G., TEM Study of Radiation Damage and Annealing of Neutron Irradiated Zirconolite, *Proc. Symp. "Sci. Bas. Nucl. Waste Management XX,"* Pittsburgh: MRS, 1996, vol. 412, pp. 329–336.

Maddrell, E.R., Effect on Conjoint Additions of Rare Earth Element Oxides on the Phase Stability of Zirconia, *Proc. Symp. "Sci. Bas. Nucl. Waste Management XX,"* Pittsburgh: MRS, 1997, vol. 412, pp. 353–360.

GOST (State Standard), *R 50089-92: Methods for Determination of Long-Term Durability of Solidified High-Level Radioactive Wastes*, 1992.

Matzke, Hj. and van Geel, J., Incorporation of Pu and Other Actinides in Borosilicate Glass and in Waste Ceramics, *Disposal of Weapon Plutonium. Netherlands*, Kluwer Acad. Publ., 1996, pp. 93–105.

Mazzi, F. and Munno, R., Calciobetafite (New Mineral of the Pyrochlore Group) and Related Minerals from Campi Flegrei, Italy; Crystal Structures of Polymignite and Zirkelite: Comparison with Pyrochlore and Zirconolite, *Am. Mineral.*, 1983, vol. 68, pp. 262–276.

Mineraly. Spravochnik (Minerals. Handbook), Chukhrov, F.V. and Bonshtedt-Kupletskaya, E.M., Eds., Moscow: Nauka, 1967, vol. 2, issue 3.

Morgan, P.E.D. and Ryerson, F.J., A New "Cubic" Crystal Compound, *J. Mater. Sci. Lett.*, 1982, vol. 1, no. 8, pp. 351–352.

Murakami, T., Chakoumakos, B.C., Ewing, R.C., *et al.*, Alpha-Decay Event Damage in Zircon, *Am. Mineral.*, 1991, vol. 76, pp. 1510–1532.

Orlova, A.I., Charlamova, A.A., and Volkov, Yu.F., Investigation of Plutonium, Americium and Curium Phosphates As a Basis for Inclusion into Kosnarite-Type Ceramic Waste Forms, in *Proc. 3rd Annual Meeting for Coordination and Review of LLNL Contract Work*, Livermore: LLNL, 2002, pp. 407–418, paper JJ 11.31, CD-version.

Radioactive Waste Forms, New York: Elsevier, 1988.

Ringwood, A.E., Disposal of High-Level Nuclear Wastes: a Geological Perspective, *Mineral. Mag.*, 1985, vol. 49, pp. 159–176.

Sinclair, W. and Ringwood, A.E., Alpha-Recoil Damage in Natural Zirconolite and Perovskite, *Geochem. J.*, 1981, vol. 15, no. 5, pp. 229–243.

Sizgek, G.D., Thermal Considerations in a Very Deep Borehole Nuclear Waste Repository for Synroc, *Proc. Symp. "Sci. Bas. Nucl. Waste Management XXIV." Warrendale*, MRS, 2001, vol. 663, pp. 819–826.

Smelova, T.V., Krylova, N.V., Yudintsev, S.V., and Nikonov, B.S., Silicate Matrix for Actinide-Bearing Wastes, *Dokl. Akad. Nauk*, 2000, vol. 374, no. 2, pp. 242–246.

Smith, K.L., Lumpkin, G.R., Blackford, M.G., and Vance, E.R., Amorphisation of Perovskite: the Effect of Composition and Pre-Existing Cation Vacancies, *Proc. Symp. "Sci. Bas. Nucl. Waste Management XXII." Warrendale*, MRS, 1999, vol. 556, pp. 1185–1191.

Smith, K.L., Zaluzec, N.J., and Lumpkin, G.R., The Relative Radiation Resistance of Zirconolite, Pyrochlore and Perovskite to 1.5 MeV Kr^+ Ions, *Proc. Symp. "Sci. Bas. Nucl. Waste Management XXI." Warrendale*, MRS, 1998, vol. 506, pp. 931–932.

Stefanovsky, S.V., Yudintsev, S.V., and Kir'yanova, O.I., Effect of Synthesis Conditions on Phase Composition of Pyrochlore–Brannerite Ceramics, *Fiz. Khim. Obrab. Mater.*, 2001, no. 5, pp. 90–98.

Stefanovsky, S.V., Yudintsev, S.V., Nikonov, B.S., *et al.*, Effect of Synthesis Condition on Phase Composition of Pyrochlore–Brannerite Ceramics, *Proc. Symp. "Sci. Bas. Nucl. Waste Management XXIV." Warrendale*, MRS, 2001_2, vol. 663, pp. 315–324.

Stefanovsky, S.V., Yudintsev, S.V., Nikonov, B.S., *et al.*, Murataite-Based Ceramics for Actinide Waste Immobilization, *Proc. Symp. "Sci. Bas. Nucl. Waste Management XXII." Warrendale*, MRS, 1999, vol. 556, pp. 121–128.

Urusov, V.S., Rusakov, V.S., and Yudintsev, S.V., Valent State and Structural Position of Fe Atoms in Synthetic Murataite, *Dokl. Akad. Nauk*, 2002, vol. 384, no. 4, pp. 527–532.

Utsunomiya, A., Wang, L.M., Yudintsev, S., and Ewing, R.C., Ion Irradiation Effects in Synthetic Garnets Incorporating Actinides, *Proc. Symp. "Sci. Bas. Nucl. Waste Management XXV." Warrendale*, MRS, 2002_1, vol. 713, pp. 495–500.

Utsunomiya S., Wang L.M., Yudintsev S., and Ewing R.C. Ion Irradiation Effects in Natural and Synthetic Garnets, *J. Nucl. Mater.*, 2002_2, no. 303, pp. 177–187.

Vance, E.R. and Metson, J.B., Radiation Damage in Natural Titanites, *Minerals,* 1985, vol. 12, pp. 255–260.

Vance, E.R., Begg, B.D., Day, R.A., and Ball, C.J., Zirconolite-Rich Ceramics for Actinide Wastes, *Proc. Symp. "Sci. Bas. Nucl. Waste Management XVIII,"* Pittsburgh: MRS, 1995, vol. 353, pp. 767–774.

Wald, J.W. and Weber, W.J., Effects of Self-Radiation Damage on the Leachability of Actinide-Host Phase, *Adv. Ceram.*, 1984, vol. 8, pp. 71–75.

Wang, L.M., Cameron, M., Weber, W.J., *et al.*, In situ TEM Observation of Radiation Induced Amorphization of Crystals with Apatite Structure, in *Hydroxyapatite and Related Materials*, CRC, 1994, pp. 243–249.

Wang, S.X., Begg, B.D., Wang, L.M., *et al.*, Radiation Stability of Gadolinium Zirconate: A Waste Form for Plutonium Disposition, *J. Mater. Res.*, 1999_1, vol. 14, no. 12, pp. 4470–4473.

Wang, S.X., Lumpkin, G.R., Wang, L.M., and Ewing, R.C., Ion Irradiation-Induced Amorphization of Six Zirconolite Compositions, *Nucl. Instr. Methods Phys. Res.*, 2000_1, section 166–167, pp. 293–298.

Wang, S.X., Wang, L.M., Ewing, R.C., *et al.*, Ion Irradiation-Induced Phase Transformation of Pyrochlore and Zirconolite., *Nucl. Instr. Methods Phys. Res.*, 1999_2, section 148, pp. 704–709.

Wang, S.X., Wang, L.M., Ewing, R.C., and Govindan Kutty, K.V., Ion Irradiation of Rare-Earth- and Yttrium-Titanate-Pyrochlores, *Nucl. Instr. Methods Phys. Res.*, 2000_2, section 169, pp. 135–140.

Weber, W.J. and Ewing, R.C., Radiation Effects in Crystalline Oxide Host Phases for the Immobilization of Actinides, *Proc. Symp. "Sci. Bas. Nucl. Waste Management XXV," Warrendale*, MRS, 2002, vol. 713, pp. 443–454.

Weber, W.J. and Roberts, F.P., A Review of Radiation Effects in Solid Nuclear Waste Forms, *Nucl. Technol.*, 1983, vol. 60, pp. 178–198.

Weber, W.J., Ewing, R.C., and Catlow, C.R.A., Radiation Effects in Crystalline Ceramics for the Immobilization of High-Level Nuclear Waste and Plutonium, *J. Mater. Res.*, 1998, vol. 13, no. 6, pp. 1434–1482.

Weber, W.J., Ewing, R.C., Angell, C.A., *et al.*, Radiation Effects in Glasses Used for Immobilization of High-Level Waste and Plutonium, *J. Mater. Res.*, 1997, vol. 12, no. 7, pp. 1946–1978.

Weber, W.J., The Effect of Radiation on Nuclear Waste Forms, *J. Miner. Met. Mater. Soc.*, 1991, vol. 43, no. 7, pp. 35–39.

Weber, W.J., Wald, J.W., and Matzke, Hj., Effects of Self-Irradiation Damage in Cm-Doped $Gd_2Ti_2O_7$ and $CaZrTi_2O_7$, *J. Nucl. Mater.*, 1986, no. 138, pp. 196–209.

White, T.J., Ewing, R.C., Wang, L.M., *et al.*, Temperature Dependence of Amorphization for Zirconolite and Perovskite Irradiated with 1 MeV Kr Ions, *Proc. Symp. "Sci. Bas. Nucl. Waste Management XVIII,"* Pittsburgh: MRS, 1995, vol. 353, pp. 1413–1420.

Yudintsev, S.V., Incorporation of U, Th, Zr, and Gd into Garnet-Structured Host, *Proc. Conf. Rad. Waste Manag. Env. Remed. ICEM' 01*, New York: ASME, 2001, CD-version.

Yudintsev, S.V., Lapina, M.I., Ptashkin, A.G., *et al.*, Uranium Accommodation into Garnet Host, *Proc. Symp. "Sci. Bas. Nucl. Waste Management XXV," Warrendale*, MRS, 2002, vol. 713, pp. 477–480.

Yudintsev, S.V., Stefanovsky, S.V., Nikonov, B.S., and Omelianenko, B.I., Phase and Chemical Stability of Murataite Containing Uranium, Plutonium, and Rare Earths, *Proc. Symp. "Sci. Bas. Nucl. Waste Management XXIV." Warrendale*, MRS, 2001, vol. 663, CD-version.

Yudintsev, S.V., Stefanovsky, S.V., and Ewing, R.C., Structural and Compositional Relationships in Titanate-Composed Ceramics for Actinide-Bearing Waste Immobilization, *Proc. Conf. Rad. Waste Manag. Env. Remed. ICEM'99*, New York: ASME, 1999, pp. 357–368.

Yudintsev, S.V., A Structural–Chemical Approach to Selecting Crystalline Matrices for Actinide Immobilization, *Geol. Rudn. Mestorozhd.,* 2003, vol. 45, no. 2, pp. 172–187.

Yudintseva, T.S., Radiation Damage of Pyrochlore-Group Mineral Structures, *Mater. godichn. sobraniya VMO*, (Materials of Annual Meeting of All-Russia Mineralogical Society), Moscow, 2002, pp. 198–199.

Ziegler, J.F., Biersack, J.P., and Littmark, U., *The Stopping and Range of Ions in Solids*, New York: Pergamon, 1985.